ine by NO synthases (NOSs), a family of enzymes that currently includes three different isoenzymes in mammals (14). The inducible isoform of NOS (iNOS or NOS2) is known to produce a relatively large amount of NO because of its Ca^{2+}-independent activity (14), and thus has been linked to numerous human pathologies, including Alzheimer disease, asthma, cancer, cerebral infarction, inflammatory bowel disease, arthritis, and endotoxin shock (15, 16). Thus, NO production by iNOS needs to be tightly regulated. iNOS activity can be controlled through the regulation of its synthesis, catalytic activity, and degradation. Once iNOS is expressed, its degradation is the most critical option left for the regulation of iNOS activity. Eissa's group (17–19) has reported that iNOS is regulated by ubiquitination and the proteasomal degradation pathway. Additionally, Kuang *et al.* (20) recently reported that iNOS interacted with SPSB2, and the half-life of iNOS was not only shortened in SPSB2-transgenic macrophages but also extended in SPSB2-deficient macrophages. These studies suggest that SPSB2 regulates the ubiquitination and proteasomal degradation of iNOS. The detailed mechanism by which SPSB2 regulates iNOS, however, and whether other proteins of the SPSB family also play a role in regulating iNOS remain to be determined.

The functions that are unique to each NOS isoform are attributed to the N-terminal region because the N-terminal regions, located before the oxygenase domain of three NOS isoforms, share remarkably low sequence homology and contain a unique domain or motif that enables each NOS isoform to interact with a specific partner (21) or to achieve a distinctive subcellular distribution (22). In the present study, we characterized various biological processes of iNOS regulation by the SPSB family of proteins that interact specifically with the N-terminal region of iNOS. Here, we report on the molecular mechanism by which the SPSB family of proteins targets iNOS to proteasomal degradation, the relative contributions of different SPSB proteins to iNOS regulation, and the physiological significance of SPSB-mediated iNOS degradation in activated macrophages.

EXPERIMENTAL PROCEDURES

Reagents—Ultra pure LPS from Salmonella Minnesota R595 (Re) was obtained from Alexis Biochemicals. 1400W and cycloheximide were from Calbiochem. Doxycycline was from Clontech. Anti-iNOS antibody was from Millipore. Anti-FLAG(M2) antibody was from Sigma. Anti-HA antibody was from Covance. Antibodies to Cul5, COX-2, and GAPDH were from Santa Cruz Biotechnology. Anti-JAK2 antibody and anti-Myc antibody were from Cell Signaling Technology. Anti-T7 antibody was from Novagen. Anti-ubiquitin antibody (FK2) was from Nippon Bio-Test Laboratories.

cDNAs and Plasmids—cDNAs for human iNOS (hiNOS) and mouse iNOS (miNOS) were kindly provided by H. Esumi and C. Nathan, respectively. cDNAs for human SPSB1 (hSPSB1), hSPSB3, and hSPSB4 were kindly provided by G. Wu (23). cDNA encoding the residues 7–263 of hSPSB2 was isolated from the positive yeast clone in yeast two-hybrid screening, and then cDNA encoding the full-length hSPSB2 was amplified by PCR with the following primers: 5′-CGCGGATCCGCCGCCATGGGCCAGACAGCTCTGGCAGGGGGCAGCAGCAGCAC-3′ and 5′-CCGGAATTCCCTGGTAGAGCAGGTAGCGCTTC-3′. The cDNAs encoding residues 1–124 and 1–500 of hiNOS were subcloned into the pGBKT7 vector (Clontech). The plasmid for expressing hiNOS carrying N27A mutation (hiNOS(N27A)) was constructed by using the QuikChange™ Site-directed Mutagenesis kit (Stratagene) and pSG5-hiNOS vector as a template. The cDNAs encoding hSPSB1, hSPSB2, hSPSB3, hSPSB4, hSPSB1ΔSB (residues 1–231), hSPSB2ΔSB (residues 1–221), and hSPSB4ΔSB (residues 1–231) were subcloned into the pEFBOSEX-FLAG vector (24). The cDNAs encoding hSPSB4, hiNOS(1–124) and hiNOS(1–124)(N27A) were subcloned into the pEFBOSEX-HA vector (24). The cDNAs encoding N-terminal Myc-tagged ubiquitin and 3xT7-tagged Elongin C were subcloned into the pMXrmv5 retroviral vector (25). The cDNAs encoding hiNOS and hiNOS(N27A) were subcloned into the pMXrmv5-$(G_4S)_3$-YFP retroviral vector (25). The cDNAs encoding hSPSB1 and hSPSB1ΔSB were subcloned into the pMXrmv5-$(G_4S)_3$-CFP retroviral vector (25). The cDNA encoding the residues 1–118 of miNOS (miNOS(1–118)) and miNOS(1–118)(N27A) with the C-terminal FLAG tag were subcloned into the pRevTRE vector (Clontech).

Generation of Stable Cell Lines—HEK293T cells expressing N-terminal Myc-tagged ubiquitin (HEK293T-^{myc}Ub cells) and N-terminal 3xT7-tagged Elongin C (HEK293T-^{3xT7}EloC cells) were prepared by retroviral gene transfer as described previously (25). The positive cells were selected for growth in medium containing 2 μg/ml puromycin for a week, and individual clones were tested by immunoblotting using an anti-Myc or an anti-T7 antibody. The DOX-regulated miNOS(1–118)^{FLAG}-expressing RAW264.7 mouse macrophage cell line (RAW-TetOFF-miNOS(1–118)^{FLAG} and -miNOS(1–118)(N27A)^{FLAG} cells) was prepared using the Rev-Tet System (Clontech). Briefly, the pRevTet-OFF vector was introduced to RAW264.7 cells by retroviral gene transfer as described previously (26). The positive cells were selected for growth in medium containing 400 μg/ml G-418 for 2 weeks. Individual clones were infected with the pRevTRE-Luc vector, and the "on-off" regulation by DOX was tested using a luciferase assay. The cells obtained at this step are referred to as RAW-TetOFF cells. Then the pRevTRE-miNOS(1–118)^{FLAG} or pRevTRE-miNOS(1–118)(N27A)^{FLAG} vector was introduced to the RAW-TetOFF cells by retroviral gene transfer and the positive cells were selected for growth in medium containing 400 μg/ml hygromycin B and 400 μg/ml G-418 for 2 weeks. The "on-off" regulation by DOX in each clone was tested by immunoblotting using an anti-FLAG antibody.

Cell Culture—HEK293T cells were grown in Dulbecco's modified Eagle's medium (DMEM) containing 10% fetal bovine serum (FBS). HEK293T-^{myc}Ub cells and HEK293T-^{3xT7}EloC cells were grown in DMEM containing 10% FBS and 1 μg/ml puromycin. RAW-TetOFF-miNOS(1–118)^{FLAG} and RAW-TetOFF-miNOS(1–118)(N27A)^{FLAG} cells were grown in RPMI containing 10% FBS, 1 mM pyruvate, 200 μg/ml G-418, 200 μg/ml hygromycin B, and 100 ng/ml DOX. When proteins of interest were induced by removing DOX from the culture medium, Tet System Approved FBS (Clontech) was used

instead of regular FBS, because regular FBS may contain tetracycline.

Yeast Two-hybrid Screening—Yeast two-hybrid screening was performed using the Matchmaker GAL4 Two-Hybrid System 3 (Clontech). The human liver, spleen, heart, fetal brain, and adult brain cDNA libraries (Clontech) were screened with amino acids 1–124 of human iNOS as the bait, following the manufacturer's instructions.

Quantitation of Nitrite in Culture Medium—The production of nitrite was measured using Griess reagent as described previously (26).

Co-immunoprecipitation—Both HEK293T cells and HEK293T-^{3xT7}EloC cells in a 6-well plate were transfected with the indicated plasmids for 24 h. The cells were lysed in 1 ml of buffer A (50 mM Tris-HCl, 150 mM NaCl, 1% Nonidet P-40, 5 mM EDTA, and a protease inhibitor mixture (Roche), pH 7.5). The lysates were centrifuged at 20,000 × *g* for 10 min at 4 °C. The supernatants were pre-cleared with 40 μl of protein G-Sepharose 4FF beads (GE Healthcare) for 30 min. The pre-cleared lysates were incubated with the indicated antibodies for 4 h to overnight at 4 °C, and successively with 40 μl of protein G-Sepharose 4FF beads for 4 h at 4 °C. The beads were washed five times with 1 ml of buffer A. Immunoprecipitated proteins were eluted by boiling with 40 μl of 2× SDS-PAGE sample buffer for 5 min, and subjected to immunoblotting.

Detection of Ubiquitinated iNOS—Either HEK293T-^{myc}Ub cells in 6-well plates, or RAW-TetOFF-miNOS(1–118)^{FLAG} and RAW-TetOFF-miNOS(1–118)(N27A)^{FLAG} cells in 6-cm dishes were washed with PBS and lysed with 1 ml of buffer B (PBS containing 0.1% SDS, 0.5% deoxycholic acid, 1% Nonidet P-40, 0.5 mM EDTA, 5 mM *N*-ethylmaleimide (NEM), 1 mM NaF, and a protease inhibitor mixture). The lysates were centrifuged at 20,000 × *g* for 20 min at 4 °C, and the supernatants were then pre-cleared with 50 μl protein G-Sepharose 4FF beads for 30 min, and centrifuged at 20,000 × *g* for 10 min at 4 °C. The pre-cleared lysates were incubated with 3 μg anti-iNOS antibody for 90 min at 4 °C, and successively with 50 μl protein G-Sepharose 4FF beads for 90 min at 4 °C. The beads were washed five times with 1 ml of buffer B. Immunoprecipitated proteins were eluted by boiling with 40 μl of 2× SDS-PAGE sample buffer for 1 min, and subjected to immunoblotting.

Microscopy—HEK293T cells transfected with the indicated plasmids were placed into a glass bottom dish (IWAKI) coated with poly-L-lysine (Sigma). The next day, images were acquired using a KEYENCE BZ-9000 or an Olympus IX-71 fluorescent microscope.

Cell Viability Assay—RAW-TetOFF-miNOS(1–118)^{FLAG} and RAW-TetOFF-miNOS(1–118) (N27A)^{FLAG} cells were washed with PBS, and then incubated with PBS containing 5 mM EDTA for 7 min. The cells were collected and stained with 100 μl of 0.25 μg/ml 7-aminoactinomycin D (7-AAD) in SB (PBS containing 1% FBS and 0.09% sodium azide) for 10 min in the dark. Then, 500 μl of SB was added to the cells, and the stained cells were analyzed by flow cytometry using FACSCalibur (BD) and FlowJo software (Tree Star).

Statistical Analysis—All data are presented as means and S.D. Probability values were based on a paired *t* test or one-way analysis of variance (ANOVA) followed by Tukey's multiple comparison test.

RESULTS

SPSB1 and SPSB4 Interact with iNOS in a D-I-N-N-N Sequence-dependent Manner and Induce Its Subcellular Redistribution in a SOCS Box-dependent Manner—To uncover the molecular mechanisms of iNOS regulation, we sought to identify proteins that interacted with the N-terminal region located before the oxygenase domain of human iNOS using yeast two-hybrid screens. Using residues 1–124 of human iNOS as the bait, we screened 3 × 10^7 independent clones from human liver, spleen, heart, fetal brain, and adult brain cDNA libraries and obtained three X-α-Gal positive clones. Sequencing analysis and Blast searches of the GenBank™ databases indicated that one of these clones encoded almost full-length SPSB2 (residues 7–263; supplemental Fig. S1). Kuang *et al.* (10, 20) recently bioinformatically identified iNOS as an SPSB2-interacting protein by searching for proteins that contained putative *Drosophila* SPSB recognition sequences ((D/E)-(I/L)-N-N-N). They showed that the D-I-N-N-N motif was present in residues 23–27 of iNOS proteins from different species and that asparagine 27 is a key residue for interacting with iNOS. They also demonstrated that SPSB1 and SPSB4, but not SPSB3, interacted with iNOS. However, whether SPSB1 and SPSB4 also recognize the D-I-N-N-N sequence remains unclear. Thus, we examined the interaction of the iNOS protein carrying the N27A mutation (iNOS(N27A)) with SPSB1 and SPSB4. In co-immunoprecipitation experiments, SPSB1 and SPSB4 interacted with wild-type iNOS, while neither interacted with the iNOS(N27A) mutant (Fig. 1*A*), suggesting that the iNOS interactions with SPSB1 and SPSB4 are regulated in the same manner as the interaction with SPSB2.

We used microscopic imaging to investigate the effects of SPSB proteins on the subcellular distribution of iNOS in living cells. We expressed iNOS fused at its C terminus to yellow fluorescent protein (YFP) and SPSB proteins fused at their C terminus to cyan fluorescent protein (CFP) in HEK293T cells, and imaged the cells using fluorescence microscopy. Both iNOS and the iNOS(N27A) mutant were localized as discrete foci scattered throughout the cytosol, while SPSB1 and the SOCS box-deleted form of SPSB1ΔSB) showed a diffuse cytosolic localization (Fig. 1*B*). Surprisingly, we found that when iNOS and SPSB1 were co-expressed, iNOS was co-localized with SPSB1 with a significant change in the subcellular distribution from dense regions to diffuse expression similar to the localization of SPSB1 (Fig. 1*C*). The subcellular redistribution of iNOS was also observed when SPSB4 was co-expressed, and, to a lesser degree, when SPSB2 was co-expressed (supplemental Fig. S2*A*). In contrast, the iNOS(N27A) mutant did not co-localize with SPSB1 and the subcellular distribution of this mutant was unchanged (Fig. 1*D*). Next, we examined whether the SOCS box was involved in the subcellular redistribution of iNOS. We found that the subcellular distribution of iNOS was unaffected by the expression of SPSB1ΔSB, despite its strong co-localization with SPSB1ΔSB (Fig. 1*E*). Instead, the subcellular distribution of SPSB1ΔSB changed substantially, from diffuse to dense regions of expression, similar to the localization of

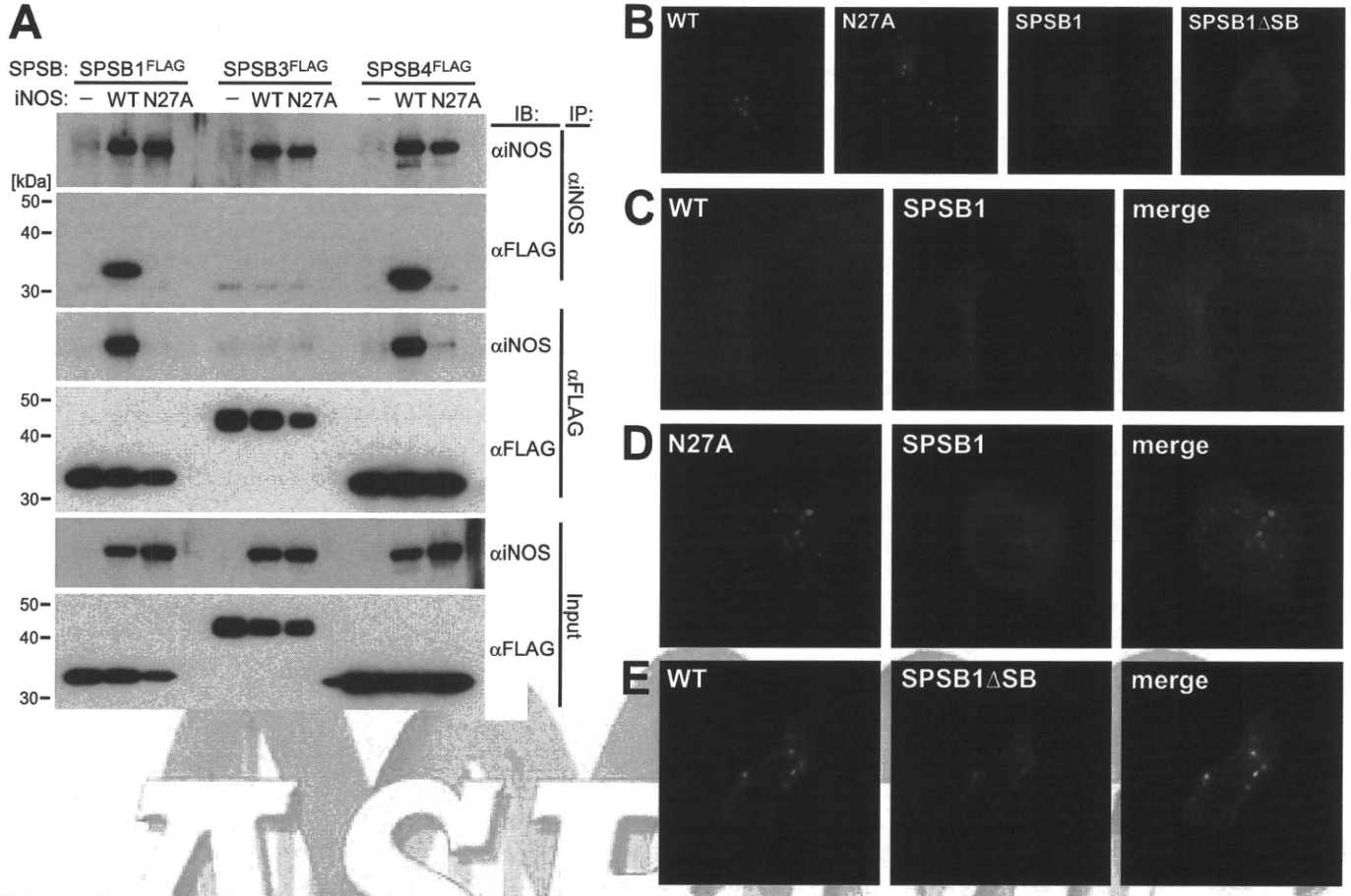

FIGURE 1. **SPSB1 and SPSB4 interact with iNOS in a D-I-N-N-N sequence-dependent manner and induce the subcellular redistribution of iNOS in a SOCS box-dependent manner.** *A*, HEK293T cells were transfected with indicated expression plasmids for 24 h. The cell lysates were prepared and subjected to immunoprecipitation and immunoblotting. *B*, in 12-well plates, HEK293T cells were transfected with an expression plasmid for iNOS-YFP, iNOS(N27A)-YFP, SPSB1-CFP, or SPSB1ΔSB-CFP for 12 h. Then the cells were placed into a 35-mm glass bottom dish. The next day, the cells were examined by fluorescence microscopy. *C–E*, HEK293T cells were transfected with expression plasmids for iNOS-YFP and SPSB1-CFP (*C*), iNOS(N27A)-YFP and SPSB1-CFP (*D*), or iNOS-YFP and SPSB1ΔSB-CFP (*E*). The cells were subjected to fluorescence microscopy as described in *B*. iNOS and iNOS(N27A) mutant are shown in *green* (pseudocolor), and SPSB1 and SPSB1ΔSB are shown in *red* (pseudocolor). Regions with co-localization appear *yellow*.

iNOS. These results suggest that an extensive subcellular redistribution of iNOS in the cytosol was caused by SPSB1 and SPSB4, and, to a lesser extent, by SPSB2, and that the SOCS box was required for this.

SPSB1 and SPSB4 Induce the Proteasomal Degradation of iNOS More Strongly than SPSB2—Although Kuang *et al.* (20) showed that SPSB2 targets iNOS for proteasomal degradation, whether SPSB1 and SPSB4 also play a role in the proteasomal degradation of iNOS remains unclear. Thus, we first examined whether iNOS levels were down-regulated by the overexpression of SPSB1 and SPSB4. We found that iNOS levels were slightly decreased when SPSB1 and SPSB4 were overexpressed, while the overexpression of SPSB2 did not affect the iNOS level (Fig. 2*A*), different from the previous observations of Kuang *et al.* We next examined whether the co-overexpression of SPSB1 and SPSB4 induced the down-regulation of iNOS more than the expression of SPSB1 or SPSB4 alone. Surprisingly, the iNOS level was unchanged in cells expressing both SPSB1 and SPSB4 compared with the control cells (Fig. 2*B*). These results led us to hypothesize that the down-regulation of iNOS is not always proportional to the expression levels of SPSB proteins. To test this, HEK293T cells in 24-well plates were transiently transfected with cDNAs expressing iNOS (200 ng) and each SPSB protein (0.01–600 ng) for 24 h, and then iNOS levels in the cells and nitrite accumulation in the cell culture medium were analyzed by immunoblotting and the Griess reaction assay, respectively. We found that both the iNOS level and nitrite accumulation decreased substantially when SPSB1 and SPSB4 were expressed by transfection with 200:1 to 200:10 ng cDNA ratios of iNOS to SPSB (Fig. 2, *C* and *D*). This effect was also observed, to a lesser degree, when SPSB2 was expressed. Surprisingly, this effect was diminished when the expression level of SPSB1 and SPSB4 was increased by transfection with 200:100 to 200:600 ng cDNA ratios of iNOS to SPSB. Additionally, this effect was completely abrogated when the expression level of SPSB2 was increased. Consistent with the degradation of iNOS, the much lower expression of SPSB2 induced the subcellular redistribution of iNOS (supplemental Fig. S2*B*). These results suggest that the molar ratio of iNOS to SPSB is important for iNOS regulation, and that SPSB1 and SPSB4 have a more potent effect on the subcellular redistribution and down-regulation of iNOS than SPSB2.

Next, to determine whether the down-regulation of iNOS was caused by accelerated degradation of iNOS, we examined

balt3/zbc-bc/zbc-bc/zbc01411/zbc5330-11z ZSUBMIT 17 xppws S=1 9/2/11 13:57 | 4/Color Figure(s) F1 | ARTNO: M110.190678

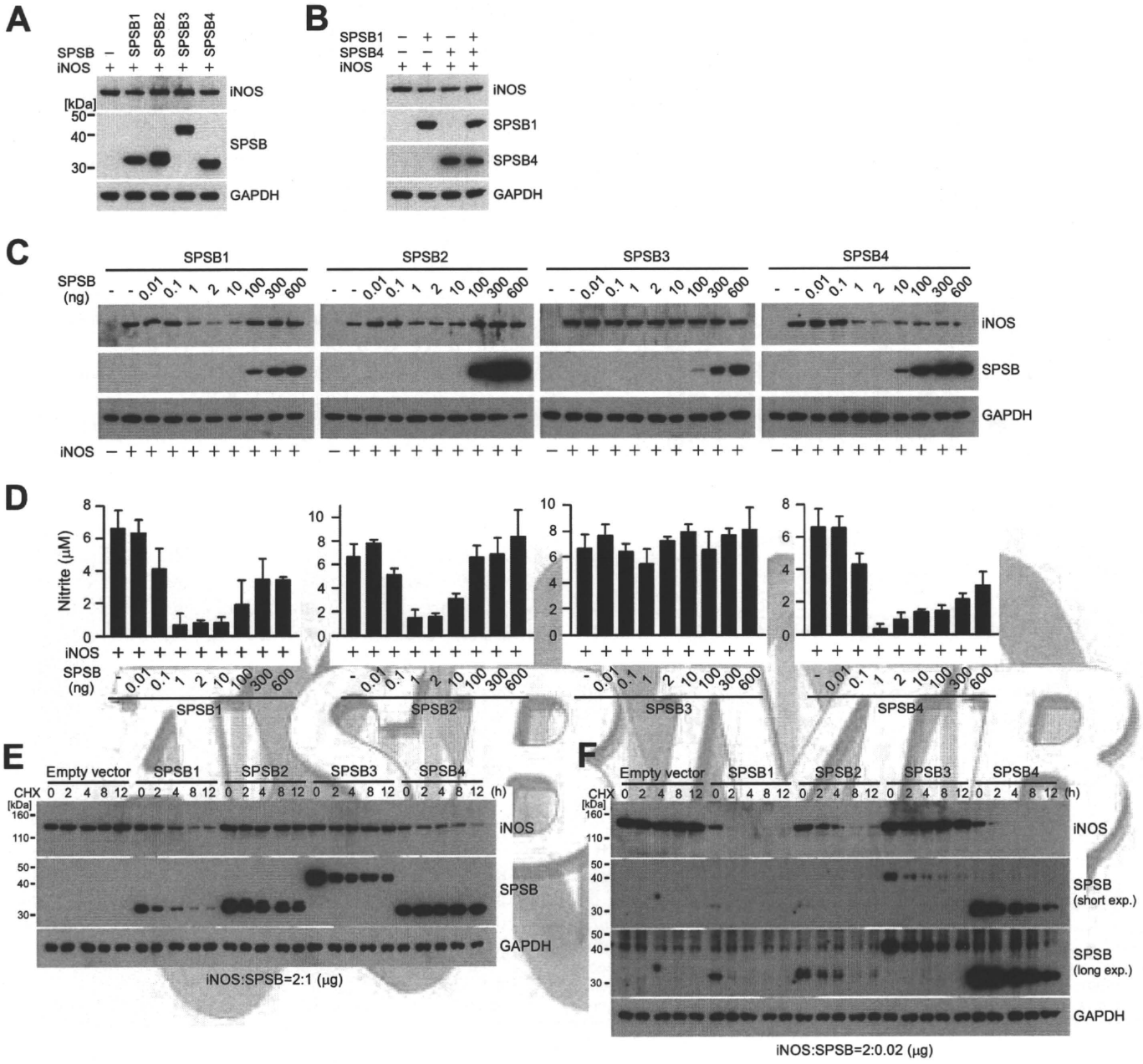

FIGURE 2. **SPSB1 and SPSB4 induce the degradation of iNOS more strongly than SPSB2.** *A*, HEK293T cells in 12-well plates were transfected with expression plasmids for iNOS (0.8 μg), FLAG-tagged SPSBs (0.2 μg), and the pEFBOSEX vector (0.6 μg) for 24 h. Then, the cell lysates were prepared, and subjected to immunoblotting. *B*, HEK293T cells in 12-well plates were transfected with expression plasmids for iNOS (0.8 μg), FLAG-tagged SPSB1 (0.2 μg), and/or HA-tagged SPSB4 (0.2 μg) for 24 h. The pEFBOSEX vector was also transfected to ensure that a total of 1.6 μg of DNA was used per transfection. Then, the cell lysates were prepared, and subjected to immunoblotting. *C* and *D*, HEK293T cells in 24-well plates were transfected with expression plasmids for iNOS (200 ng) and FLAG-tagged SPSBs (0.01–600 ng) for 24 h. The pEFBOSEX vector was also transfected to ensure that a total of 800 ng of DNA was used per transfection. Then, the cell lysates were prepared, and subjected to immunoblotting (*C*). In addition, concentration of nitrite in the cell culture medium was assessed by the Griess assay (*D*). Data represent mean ± S.D., $n = 3$. *E* and *F*, HEK293T cells in 6-well plates were transfected with expression plasmids for iNOS and FLAG-tagged SPSBs at the indicated ratio of iNOS to SPSBs for 12 h. Then the cells were placed into 5 wells of 24-well plate. After 12 h, the cells were treated with 100 μM CHX for the indicated periods. The cell lysates were prepared and subjected to immunoblotting.

the stability of iNOS protein in cycloheximide (CHX) chase assays (27). We found that SPSB1 and SPSB4, but not SPSB2, triggered iNOS degradation in cells transfected with cDNAs at a 2:1 μg ratio of iNOS to SPSB (Fig. 2*E*). Consistent with the results in Fig. 2, *C* and *D*, the much lower expression of SPSB1 and SPSB4 by transfection with cDNAs at a 2:0.02 μg ratio of iNOS to SPSB induced more rapid degradation of iNOS (Fig. 2*F*) that was abolished in cells treated with the proteasome inhibitor MG-132 (supplemental Fig. S3), indicating that both SPSB1 and SPSB4 target iNOS for proteasomal degradation. The lower expression of SPSB2 also triggered iNOS degradation, but this degradation was much weaker than that mediated by SPSB1 and SPSB4.

To determine whether the physical interaction between iNOS and SPSB proteins is necessary for the down-regulation of iNOS, we performed the same experiments using the iNOS(N27A) mutant. We found that, in contrast to wild-type iNOS, the levels of the iNOS(N27A) mutant and NO produc-

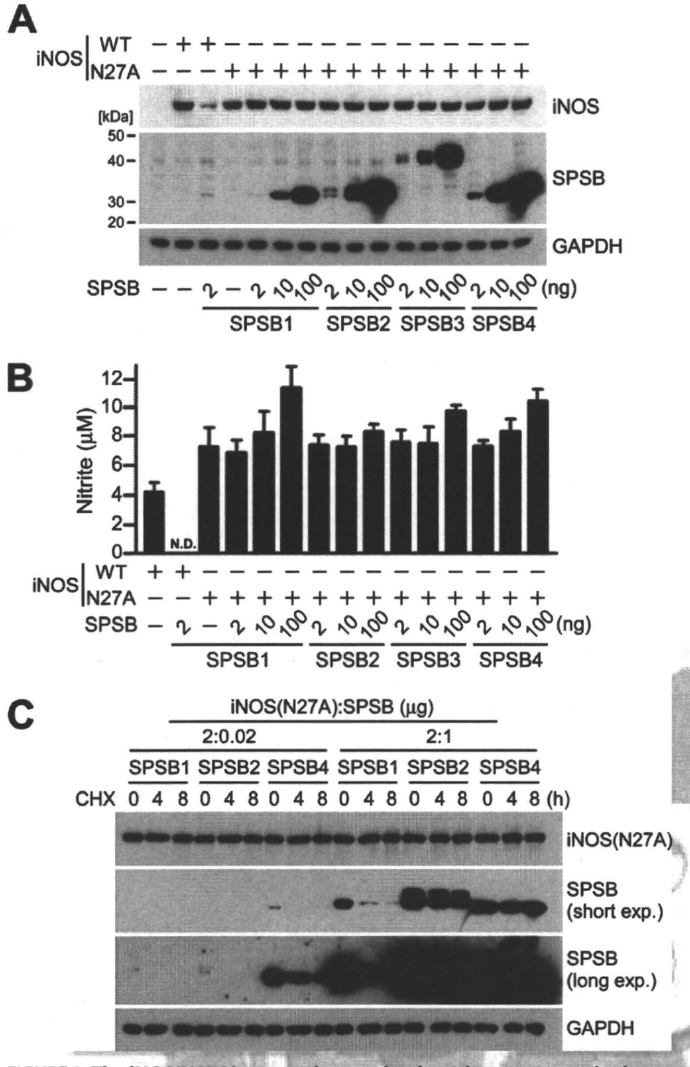

FIGURE 3. **The iNOS(N27A) mutant is completely resistant to protein degradation mediated by SPSB1, SPSB2, and SPSB4.** *A* and *B*, HEK293T cells in 24-well plates were transfected with expression plasmids for the iNOS(N27A) mutant (200 ng) and FLAG-tagged SPSBs (2–100 ng) for 24 h. The pEFBOSEX vector was also transfected to ensure that a total of 800 ng of DNA was used per transfection. Then, the levels of the iNOS(N27A) mutant and concentration of nitrite in the cell culture medium were determined as described in the legend to Fig. 2, *C* and *D*. Data represent mean ± S.D., $n = 3$. *C*, HEK293T cells in 6-well plates were transfected with expression plasmids for the iNOS(N27A) mutant and FLAG-tagged SPSBs at the indicated ratio of the iNOS(N27A) mutant to SPSBs for 12 h. Then the cells were placed into 3 wells of 24-well plate. After 12 h, the cells were treated with 100 μM CHX for the indicated periods. The cell lysates were prepared, and subjected to immunoblotting.

tion via this mutant were not affected by the expression of any of the SPSB proteins (Fig. 3, *A* and *B*). Additionally, the lifetime of the iNOS(N27A) mutant was unchanged by SPSB1, SPSB2, and SPSB4 (Fig. 3*C*), demonstrating that the iNOS(N27A) mutant is resistant to protein degradation mediated by these SPSB proteins.

SPSB1 and SPSB4 Induce the Ubiquitination of iNOS More Potently than SPSB2—Because SPSB1 and SPSB4 have more potent effects on the proteasomal degradation of iNOS than SPSB2, we next investigated the relative contributions of SPSB1, SPSB2, and SPSB4 to iNOS ubiquitination. To evaluate the level of ubiquitinated iNOS, HEK293T cells stably expressing Myc-tagged ubiquitin were transfected with cDNAs expressing iNOS and SPSB proteins for 24 h, followed by treatment with MG-132 for 4 h to accumulate ubiquitinated proteins. iNOS was immunoprecipitated with an iNOS antibody, and then the levels of ubiquitinated iNOS were analyzed by immunoblotting using a Myc antibody. We confirmed the expression of transfected iNOS and SPSB proteins by immunoblotting (Fig. 4*A*). We found that the level of ubiquitinated iNOS was enhanced, 4.6-, 2.9-, and 5.6-fold in cells transfected with SPSB1, SPSB2, and SPSB4, respectively (Fig. 4, *B* and *C*). These results indicate that, consistent with the degradation of iNOS, SPSB1 and SPSB4 induce the ubiquitination of iNOS more potently than SPSB2. F4

SPSB1, SPSB2, and SPSB4 Form a Bridge between iNOS and the Elongin C-Cul5 E3 Ubiquitin Ligase Complex—It has been shown that SOCS box-containing proteins interact with Elongin C and Cul5, components of the ECS E3 ubiquitin ligase complex (7), suggesting that SOCS box-containing proteins may be substrate recognition subunits of the ECS E3 ubiquitin ligase complex that polyubiquitinates substrate proteins, targeting them for proteasomal degradation. However, no direct evidence indicates that SPSB proteins mediate the interaction between the substrate and the ECS E3 ubiquitin ligase complex. Thus, we examined whether SPSB1, SPSB2, and SPSB4 mediate the iNOS interactions with Elongin C and Cul5. HEK293T cells stably expressing 3×T7-tagged Elongin C were transfected with cDNAs expressing iNOS and SPSB proteins. iNOS was immunoprecipitated with an iNOS antibody, and then the interaction with iNOS was analyzed by immunoblotting. We confirmed the expression of transfected iNOS, SPSB, and Elongin C by immunoblotting (Fig. 5*A*). We found that both Elongin C and endogenous Cul5 were co-immunoprecipitated with iNOS when SPSB1, SPSB2, and SPSB4 were expressed (Fig. 5*B*). In contrast, SPSB3 and SPSBΔSB mutants could not mediate the iNOS interactions with Elongin C and Cul5, probably because of their respective inability to interact with iNOS and Elongin C/Cul5. Next, we immunoprecipitated Elongin C with a T7 antibody and analyzed the interaction of iNOS with Elongin C by immunoblotting. We found that iNOS was co-immunoprecipitated with Elongin C when SPSB1, SPSB2, and SPSB4 were expressed (Fig. 5*C*). In contrast, SPSB3 could not mediate an interaction between Elongin C and iNOS, although SPSB3 was co-immunoprecipitated with Elongin C. The SPSBΔSB mutants were not co-immunoprecipitated with Elongin C, because they lack a SOCS box. These results demonstrate that SPSB1, SPSB2, and SPSB4 form a bridge between iNOS and the ECS E3 ubiquitin ligase complex in a SOCS box-dependent manner. F5

The N-terminal Fragment of iNOS Could Inhibit iNOS Degradation by Disrupting iNOS-SPSB Interactions—Cell and tissue microarray expression data mined from the Genomic Institute of the Novartis Research Foundation (GNF) indicated that SPSB1, SPSB2, and SPSB4 mRNAs are broadly expressed in various murine cell types and tissues (supplemental Fig. S4). We also confirmed by reverse transcription-polymerase chain reaction (RT-PCR) that both SPSB1 and SPSB2 mRNAs were expressed in cells of the mouse macrophage cell line RAW264.7 (supplemental Fig. S5). These results suggest that SPSB1, SPSB2, and SPSB4 may compensate for each of the other's loss of function if the expression of a certain SPSB is lost, as a result ZSI ZSI

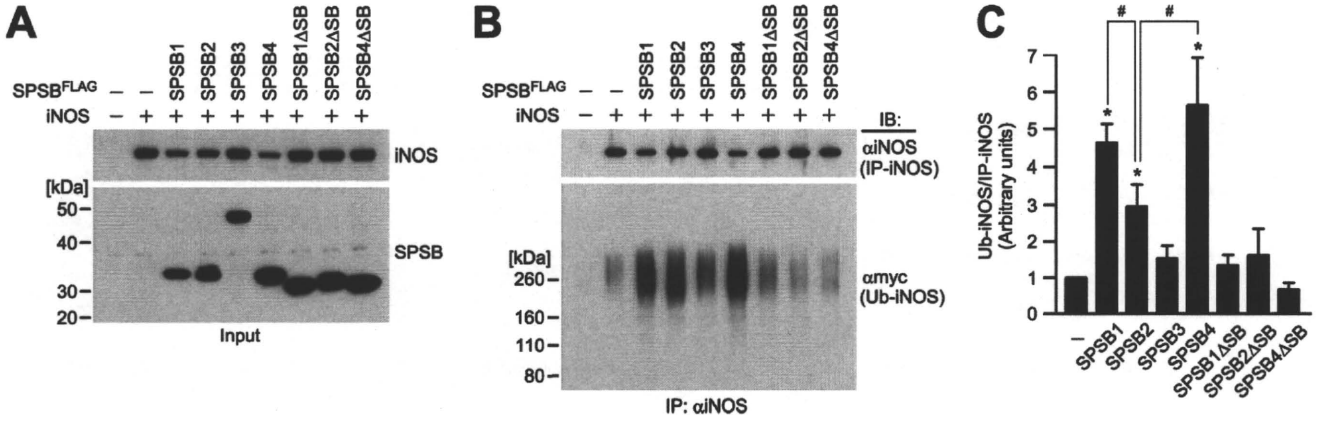

FIGURE 4. **SPSB1 and SPSB4 induce the ubiquitination of iNOS more potently than SPSB2.** *A* and *B*, In 6-well plates, HEK293T cells stably expressing Myc-tagged ubiquitin were transfected with expression plasmids for iNOS (2 μg) and FLAG-tagged SPSB (20 ng) for 24 h followed by treatment with 5 μM MG-132 for 4 h. Part of each cell lysate was subjected to immunoblotting (*A*). The remaining part of each cell lysate was subjected to immunoprecipitation using an anti-iNOS antibody, and the ubiquitinated iNOS was analyzed by immunoblotting using an anti-Myc antibody (*B*). *C*, quantification of the levels of ubiquitinated iNOS shown in *B*. Data represent mean ± S.D., $n = 3$. *, $p < 0.05$, compared with samples from cells not transfected with SPSB. #, $p < 0.05$, compared with samples from cells transfected with SPSB2.

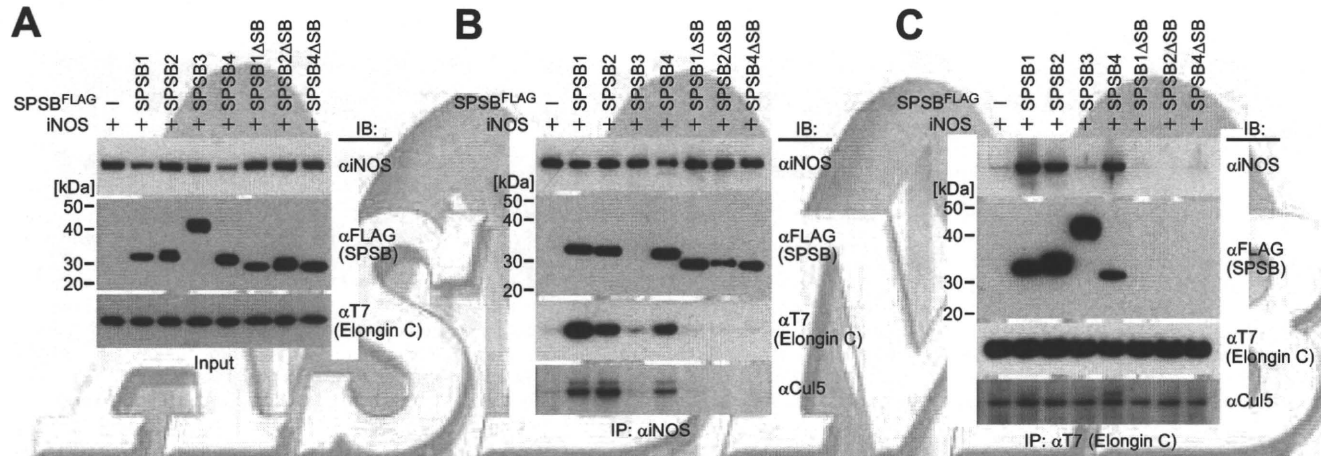

FIGURE 5. **iNOS binds to Elongin C and Cul5 via SPSB1, SPSB2, and SPSB4.** In 6-well plates, HEK293T cells stably expressing 3xT7-tagged Elongin C were transfected with expression plasmids for iNOS (2 μg) and FLAG-tagged SPSB (0.5 μg) for 24 h. The cell lysates were prepared and part of each cell lysate was subjected to immunoblotting (*A*). The remaining part of each cell lysate was subjected to immunoprecipitation using an anti-iNOS antibody (*B*) and an anti-T7 antibody (*C*). Then, immunoblotting was carried out using the indicated antibodies.

of siRNA or gene knock-out. To investigate the biochemical and physiological significance of SPSB1, SPSB2, and SPSB4 during iNOS induction in macrophages, we attempted to disrupt iNOS-SPSB interactions by overexpression of the iNOS N-terminal fragments containing a D-I-N-N-N motif, because 1) the interaction between iNOS and SPSB proteins is crucial for iNOS degradation, 2) similar to full-length iNOS, the iNOS N-terminal fragment, such as residues 1–124 of human iNOS, could interact with SPSB1, SPSB2, and SPSB4, and thus would both compete with full-length iNOS for interaction with these SPSB proteins to prevent the degradation of iNOS, and 3) it is much easier to express iNOS N-terminal fragments in macrophages than to introduce siRNAs against multiple gene targets into cells or to generate multiple gene knock-out mice. As expected, the overexpression of 1–124 iNOS fragments disrupted iNOS interactions with SPSB1, SPSB2, and SPSB4 (Fig. 6*A*) and prevented both iNOS degradation and a decrease in iNOS-mediated NO production (Fig. 6, *B* and *C*). In contrast, the 1–124 iNOS fragments carrying the N27A mutation did not alter the down-regulation of iNOS and a decrease in NO production mediated by SPSB1, SPSB2, and SPSB4 (Fig. 6, *D* and *E*, and data not shown). These results indicate that the iNOS N-terminal fragment acted as an inhibitor of SPSB1, SPSB2, and SPSB4.

Disruption of iNOS-SPSB Interactions Attenuates iNOS Ubiquitination and Prolongs the Lifetime of iNOS in Lipopolysaccharide (LPS)-activated Macrophages—To determine the biochemical and physiological significance of SPSB1, SPSB2, and SPSB4 during iNOS induction in macrophages, we established RAW-TetOFF-miNOS(1–118)^{FLAG} cells in which the mouse iNOS N-terminal fragment (residues 1–118) was reversibly expressed by a tetracycline-inducible system (residues 1–118 of mouse iNOS correspond to residues 1–124 of human iNOS). We found that the iNOS level reached its peak within 12 h of LPS stimulation and was sustained for up to at least 48 h in cells expressing the 1–118 iNOS fragments, whereas the iNOS level in the control cells reached its peak within 6 h of LPS stimulation and then declined (Fig. 7*A*). We also examined the levels of COX-2, JAK-2, and GAPDH as controls. COX-2 is an LPS-inducible protein similar to iNOS, JAK-2 is degraded

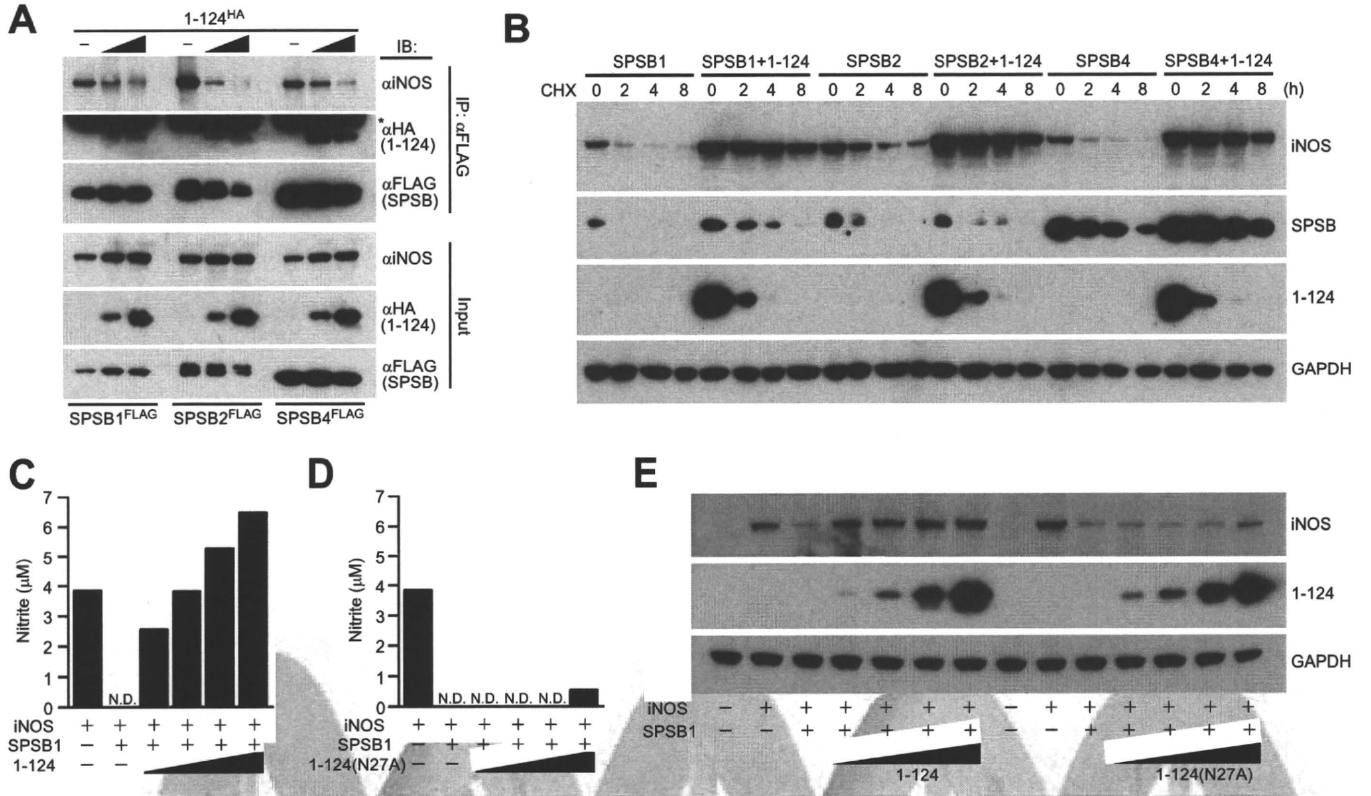

FIGURE 6. **The iNOS N-terminal fragment acts as an inhibitor of SPSB1, SPSB2, and SPSB4.** *A*, HEK293T cells in 6-well plates were transfected with expression plasmids for iNOS (1 μg), FLAG-tagged SPSB (20 ng), and HA-tagged 1–124 iNOS fragment (0, 1, and 3 μg) for 24 h followed by treatment with 5 μM MG-132 for 4 h. The cell lysates were prepared and subjected to immunoprecipitation and immunoblotting. A star indicates the light chain of the antibody. *B*, HEK293T cells in 6-well plates were transfected with expression plasmids for iNOS (2 μg), FLAG-tagged SPSB (20 ng), and HA-tagged 1–124 iNOS fragment (2 μg) for 12 h. Then the cells were placed into 4 wells of 24-well plate. After 12 h, the cells were treated with 100 μM CHX for the indicated periods. The cell lysates were prepared and subjected to immunoblotting. *A*~*B*, the pEFBOSEX vector was also transfected to ensure that a total of 4 μg of DNA was used per transfection. *C*~*E*, HEK293T cells in 24-well plates were transfected with expression plasmids for iNOS (200 ng), a FLAG-tagged SPSB (2 ng), and either an HA-tagged 1–124 iNOS fragment or an HA-tagged 1–124(N27A) iNOS fragment (50, 100, 200, and 600 ng) for 24 h. Then nitrite accumulation in the cell culture medium was assessed by the Griess assay (*C* and *D*). *N.D.*: not detected. The cell lysates were prepared from the cells shown in *C* and *D*, and were subjected to immunoblotting (*E*). *C*~*E*, pEFBOSEX vector was also transfected to ensure that a total of 800 ng of DNA was used per transfection.

under the control of another SOCS box protein, SOCS1 (28), and GAPDH is a typical internal control for immunoblotting. The kinetics of expression for each control protein were almost identical in the absence and presence of the 1–118 iNOS fragment. Consistent with sustained iNOS levels, nitrite accumulation in response to LPS stimulation was substantially elevated in the cell culture medium of cells expressing the 1–118 fragments (Fig. 7*B*). Next, we performed CHX chase assays to examine the lifetime of iNOS in LPS-activated RAW264.7 macrophages. We found that the lifetime of iNOS in cells expressing the 1–118 fragments was markedly prolonged, whereas the lifetime of control proteins was unchanged (Fig. 7*C*). We further examined the level of ubiquitinated iNOS 12 h after LPS stimulation of RAW264.7 macrophages. We found that the level of ubiquitinated iNOS was greatly diminished by the expression of the 1–118 fragments (Fig. 7, *D* and *E*). We confirmed the specificity of the 1–118 iNOS fragment to SPSB proteins and the inhibitory effect of this fragment on SPSB proteins using cells expressing the 1–118 iNOS fragment carrying the N27A mutation (1–118(N27A); supplemental Fig. S6, *A*–*E*). These results demonstrate that SPSB1, SPSB2, and SPSB4 negatively regulate the lifetime of iNOS by promoting its ubiquitination and proteasomal degradation in LPS-activated macrophages.

SPSB1, SPSB2, and SPSB4 Prevent the Cytotoxic Effect of iNOS in LPS-activated Macrophages—Because excessive amounts of NO produced via iNOS can result in cytotoxicity and apoptosis mediated by NO reactions with proteins and nucleic acids (29), we assessed NO-induced cell death 48 h after LPS stimulation of RAW264.7 macrophages. We found that nearly 70% of RAW264.7 cells expressing the 1–118 fragments were 7-AAD positive cells (dead cells), but this cytotoxic effect was almost completely abolished in cells treated with the iNOS inhibitor 1400W (30) (Fig. 7, *F* and *G*), suggesting that cell death was caused by iNOS-derived NO. In contrast, despite LPS stimulation, NO-induced cytotoxicity was not observed in control cells and cells expressing the 1–118(N27A) fragments (supplemental Fig. S6, *F* and *G*). These results indicate that SPSB1, SPSB2, and SPSB4 play an essential role in protection against the cytotoxic effect of iNOS in LPS-activated macrophages.

DISCUSSION

The three NOS isoforms have several distinct characteristics, some of which depend on the N-terminal short region located before the oxygenase domain, because this region contains a domain or motif that is unique to each NOS isoform and thus endows each NOS isoform with specific biochemical and phys-

balt3/zbc-bc/zbc-bc/zbc01411/zbc5330-11z ZSUBMIT 17 xppws S=1 9/2/11 13:57 | 4/Color Figure(s) F1 | ARTNO: M110.190678

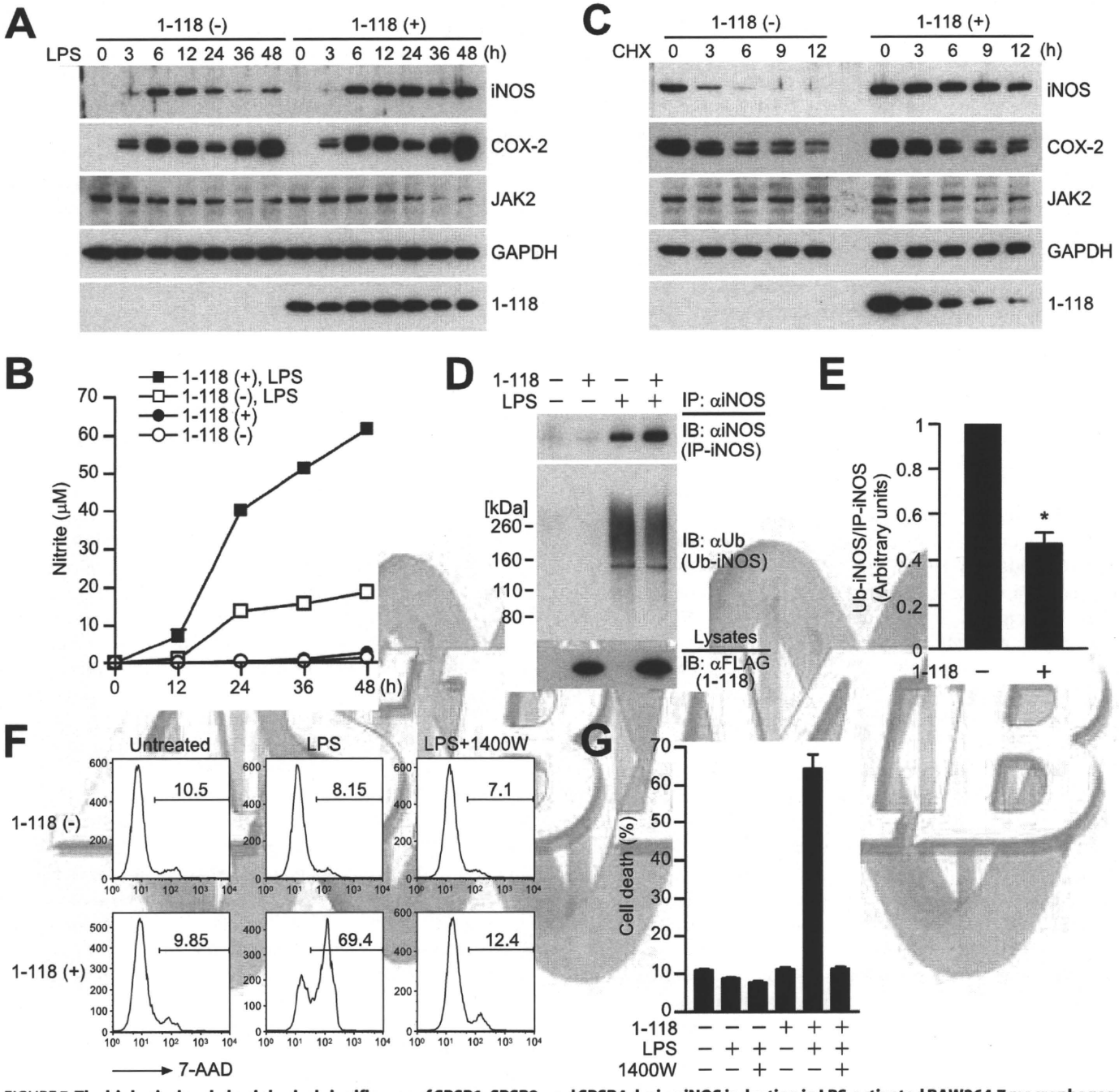

FIGURE 7. **The biological and physiological significance of SPSB1, SPSB2, and SPSB4 during iNOS induction in LPS-activated RAW264.7 macrophages.** *A*, 1–118 iNOS fragment was expressed by removing doxycycline (*DOX*) from the culture media of RAW-TetOFF-miNOS(1–118)^{FLAG} cells for 24 h. Then the cells were stimulated with 10 ng/ml LPS for the indicated periods. The cell lysates were prepared and subjected to immunoblotting. *B*, cells were treated as described in *A*, and cell culture supernatants were collected at the indicated time points. Then nitrite accumulation in the supernatants was assessed by the Griess assay. *C*, 1–118 iNOS fragment was expressed as described in *A*. Then the cells were stimulated with 10 ng/ml LPS for 12 h followed by treatment with 100 μM CHX for the indicated periods. The cell lysates were prepared and subjected to immunoblotting. *D*, 1–118 iNOS fragment was expressed as described in *A*. Then the cells were stimulated with 10 ng/ml LPS for 12 h followed by treatment with 5 μM MG-132 for 4 h. The cell lysates were prepared and subjected to immunoprecipitation using an anti-iNOS antibody. Immunoprecipitants were then subjected to immunoblotting with an anti-ubiquitin antibody to visualize the ubiquitinated iNOS. *E*, level of ubiquitinated iNOS shown in *D* was quantified as a ratio of the density of anti-ubiquitin immunoblotting (Ub-iNOS) *versus* anti-iNOS immunoblotting (IP-iNOS). Data represent mean ± S.D., $n = 3$. *, $p < 0.05$. *F*, 1–118 iNOS fragment was expressed as described in *A*. Then the cells were treated with 10 ng/ml LPS with or without 100 μM 1400W for 48 h. Cells were collected and cell viability was analyzed by 7-AAD staining. *G*, quantification of cell viability shown in *F*. Data represent mean ± S.D., $n = 3$.

iological features (21, 22). Here, we present studies examining the intrinsic mechanisms of iNOS regulation by identifying and characterizing proteins that interact specifically with the N-terminal region of iNOS. Our results reveal that SPSB1, SPSB2, and SPSB4 interact with the N-terminal region of iNOS, induce the subcellular redistribution of iNOS, and form a bridge between iNOS and the ECS E3 ubiquitin ligase complex to target iNOS for ubiquitin/proteasome-dependent degradation. SPSB1 and SPSB4 have greater effects on these biological processes of iNOS regulation than SPSB2. The negative regulation of iNOS by these SPSB proteins contributes importantly to protection against the cytotoxic effect of iNOS in activated macrophages.

iNOS Regulation by the ECS(SPSB1/2/4) E3 Ubiquitin Ligases

Although more than 50 SOCS box-containing proteins have been found and are thought to act as substrate recognition subunits of the ECS E3 ubiquitin ligase complex, only a few substrates for SOCS box-containing proteins have been identified. Our observation that iNOS was clearly immunoprecipitated with Elongin C and Cul5 in the presence of SPSB1, SPSB2, and SPSB4 is the first direct evidence that the SPSB family of proteins links the substrate with the ECS E3 ubiquitin ligase complex. The bioinformatic analysis by Kuang *et al.* (20) reported that 11 mouse and 16 human proteins contained the (D/E)-(I/L)-N-N-N sequence, suggesting that those proteins may also be regulated by SPSB1, SPSB2, and SPSB4. Future analysis of those proteins using the experimental systems described here may identify new substrates of SPSB1, SPSB2, and SPSB4, and contribute significantly to understanding the physiological roles of these SPSB proteins.

The few studies that have investigated the subcellular localization of iNOS have provided diverse findings. iNOS has been reported to reside in cells as a diffuse cytosolic protein (31) and vesicles of 50–80 nm in size (32) or to be localized in the perinuclear region (33) and Golgi apparatus (31). It has recently been reported that iNOS forms the aggresome with Hsc70, the C terminus of Hsp70-interacting proteins (CHIP), histone deacetylase 6, and dynein (34). Our results showed that the vesicle/aggresome-like localization of iNOS-YFP proteins was changed dramatically to a diffuse cytosolic localization by SPSB1, SPSB2, and SPSB4 (Fig. 1*C* and supplemental Fig. S2). SPSB1, SPSB2, and SPSB4 may access iNOS in the vesicles/aggresomes to direct the subcellular redistribution of iNOS that may be dependent on the subcellular localization of Elongin C and/or Cul5 because the SPSB1ΔSB mutant could not induce the subcellular redistribution and ubiquitin/proteasome-dependent degradation of iNOS despite strong co-localization with iNOS. The morphological patterns of iNOS localization may also be dependent on the expression levels of iNOS and SPSB proteins in each cell type, because the molar ratio of iNOS to SPSB is important for iNOS regulation (Fig. 2 and supplemental Fig. S2*B*).

We consistently observed a weak effect of SPSB2 on iNOS regulation regarding the subcellular redistribution and ubiquitin/proteasome-dependent degradation compared with the effects of SPSB1 and SPSB4. A binding affinity analysis using the SPRY domains of human SPSB1–4 together with human Par-4 peptide recently demonstrated that the binding affinity of SPSB2 to Par-4 was far inferior to those of SPSB1 and SPSB4 (35). Consistent with this, we found that despite the highest co-immunoprecipitation efficiency of SPSB2 with Elongin C, iNOS was co-immunoprecipitated less with Elongin C in cells expressing SPSB2 than in cells expressing SPSB1 and SPSB4 (Fig. 5*C*), suggesting that the binding affinity of SPSB2 to iNOS might also be weaker than those of SPSB1 and SPSB4. The detailed mechanism responsible for the weak binding affinity of SPSB2 is not clear presently, but the cause may be the lower sequence conservation of SPSB2 relative to SPSB1 and SPSB4.

Intriguingly, iNOS was significantly degraded in the presence of quite low levels of SPSB proteins, but this effect was diminished when the expression level of SPSB proteins was increased. These results indicate that iNOS degradation is not always proportional to the expression level of SPSB proteins. Unlike the single molecule E3 ubiquitin ligase, the activity of the multiprotein E3 ubiquitin ligase complex is likely to be affected by the expression level of each component, especially the substrate recognition subunit, as with SPSB proteins. This is because in the presence of excessive levels of SPSB proteins, Elongin C and Cul5 may be saturated by SPSB proteins, and free SPSB proteins may capture the substrate before the substrate interacts with the ECS-SPSB complex, and eventually SPSB proteins stabilize the substrate. Indeed, we observed that the iNOS level was significantly increased when SPSB2 was overexpressed in LPS-activated RAW264.7 macrophages (data not shown). Interestingly, mRNA expression data from GNF indicated that the mRNA expression levels of SPSB2 and SPSB4 were decreased markedly after stimulation with LPS in both bone marrow-derived macrophages and thioglycolate-elicited peritoneal macrophages (supplemental Fig. S4). Additionally, Kuang *et al.* (20) found that SPSB2 mRNA was greatly downregulated after LPS+IFN-γ treatment in bone marrow-derived macrophages. Thus, our results and those observations suggest that LPS(+IFN-γ)-induced down-regulation of SPSB proteins might facilitate the proteasomal degradation of iNOS in cells expressing high levels of SPSB proteins under basal conditions.

We still detected ubiquitinated iNOS in LPS-activated RAW264.7 macrophages expressing iNOS N-terminal fragments, although it was less than half of that observed in control cells (Fig. 7, *D* and *E*). The causes for this observation may be that the iNOS N-terminal fragments could not completely disrupt iNOS-SPSB interactions, and that other E3 ubiquitin ligases are involved in the proteasomal degradation of iNOS. Regarding the latter, it has recently been reported that CHIP, a U-box-type E3 ubiquitin ligase (36), promotes the proteasomal degradation of iNOS (34, 37). Unlike the direct interaction between iNOS and SPSB proteins, the interaction between iNOS and CHIP is mediated by Hsp70 (34), not the D-I-N-N-N sequence, suggesting that CHIP can interact with the iNOS(N27A) mutant as well as wild-type iNOS, and mediate the proteasomal degradation of this mutant. Because the iNOS(N27A) mutant is completely resistant to protein degradation mediated by ECS(SPSB1/2/4), the extent to which other E3 ubiquitin ligases, such as CHIP, are involved in the proteasomal degradation of iNOS could be determined by the degree of degradation of the iNOS(N27A) mutant. Future studies using iNOS(N27A) knock-in mice will provide important insight not only into the physiological significance of the ECS(SPSB1/2/4) E3 ubiquitin ligase complexes during iNOS induction, but also the contribution of other E3 ubiquitin ligases to the proteasomal degradation of iNOS in each cell type and tissue.

NO production by iNOS in activated macrophages is considered to be essential for various bactericidal and tumoricidal functions (38, 39). Macrophages themselves, however, are also a target of NO by an autocrine action. Indeed, excessive NO production via iNOS has been shown to induce apoptotic cell death of activated macrophages (40–42), which may allow some bacteria to survive in the host and exacerbate inflammation at the infection site (43). In RAW264.7 macrophages, LPS stimulation did not induce cell death for up to at least 48 h, whereas in

RAW264.7 macrophages expressing the iNOS N-terminal fragments to disrupt iNOS-SPSB interactions, LPS stimulation caused substantial NO-dependent cell death (Fig. 7, *F* and *G*), demonstrating the intrinsic mechanism mediated by SPSB proteins for protection against the cytotoxic effect of iNOS in activated macrophages. Clearly, much remains to be learned regarding how SPSB proteins regulate the balance of bactericidal and tumoricidal effects *versus* the cytotoxic effect of iNOS in activated macrophages.

In summary, our results indicate that iNOS is a common substrate for SPSB1, SPSB2, and SPSB4, all of which link iNOS and the ECS E3 ubiquitin ligase complex. SPSB1 and SPSB4 have more potent effects on various biological processes of iNOS regulation than SPSB2. SPSB1, SPSB2, and SPSB4 negatively regulate NO production and limit cellular toxicity through rapid ubiquitination and proteasomal degradation of iNOS in activated macrophages. A better understanding of the physiological significance of iNOS regulation by these SPSB proteins could lead to new therapeutic strategies for many disorders in which iNOS-derived excessive NO is implicated.

Acknowledgments—We thank H. Esumi for plasmid encoding human iNOS; C. Nathan for mouse iNOS; and G. Wu for human SPSB1, SPSB3, and SPSB4.

REFERENCES

1. Havens, C. G., Ho, A., Yoshioka, N., and Dowdy, S. F. (2006) *Mol. Cell. Biol.* **26,** 4701–4711
2. Schwartz, L. M., Myer, A., Kosz, L., Engelstein, M., and Maier, C. (1990) *Neuron* **5,** 411–419
3. Park, S. H., Bolender, N., Eisele, F., Kostova, Z., Takeuchi, J., Coffino, P., and Wolf, D. H. (2007) *Mol. Biol. Cell* **18,** 153–165
4. Murata, S., Sasaki, K., Kishimoto, T., Niwa, S., Hayashi, H., Takahama, Y., and Tanaka, K. (2007) *Science* **316,** 1349–1353
5. Hershko, A., and Ciechanover, A. (1998) *Annu. Rev. Biochem.* **67,** 425–479
6. Kile, B. T., Schulman, B. A., Alexander, W. S., Nicola, N. A., Martin, H. M., and Hilton, D. J. (2002) *Trends Biochem. Sci* **27,** 235–241
7. Kamura, T., Maenaka, K., Kotoshiba, S., Matsumoto, M., Kohda, D., Conaway, R. C., Conaway, J. W., and Nakayama, K. I. (2004) *Genes Dev.* **18,** 3055–3065
8. Hilton, D. J., Richardson, R. T., Alexander, W. S., Viney, E. M., Willson, T. A., Sprigg, N. S., Starr, R., Nicholson, S. E., Metcalf, D., and Nicola, N. A. (1998) *Proc. Natl. Acad. Sci. U.S.A.* **95,** 114–119
9. Nicholson, S. E., and Hilton, D. J. (1998) *J. Leukoc. Biol.* **63,** 665–668
10. Woo, J. S., Suh, H. Y., Park, S. Y., and Oh, B. H. (2006) *Mol. Cell* **24,** 967–976
11. Masters, S. L., Yao, S., Willson, T. A., Zhang, J. G., Palmer, K. R., Smith, B. J., Babon, J. J., Nicola, N. A., Norton, R. S., and Nicholson, S. E. (2006) *Nat. Struct. Mol. Biol.* **13,** 77–84
12. Bogdan, C. (2001) *Nat. Immunol.* **2,** 907–916
13. Ricciardolo, F. L., Sterk, P. J., Gaston, B., and Folkerts, G. (2004) *Physiol. Rev.* **84,** 731–765
14. Griffith, O. W., and Stuehr, D. J. (1995) *Annu. Rev. Physiol.* **57,** 707–736
15. Guo, F. H., Comhair, S. A., Zheng, S., Dweik, R. A., Eissa, N. T., Thomassen, M. J., Calhoun, W., and Erzurum, S. C. (2000) *J. Immunol.* **164,** 5970–5980
16. Nathan, C. (1997) *J. Clin. Invest.* **100,** 2417–2423
17. Musial, A., and Eissa, N. T. (2001) *J. Biol. Chem.* **276,** 24268–24273
18. Kolodziejski, P. J., Musial, A., Koo, J. S., and Eissa, N. T. (2002) *Proc. Natl. Acad. Sci. U.S.A.* **99,** 12315–12320
19. Kolodziejski, P. J., Koo, J. S., and Eissa, N. T. (2004) *Proc. Natl. Acad. Sci. U.S.A.* **101,** 18141–18146
20. Kuang, Z., Lewis, R. S., Curtis, J. M., Zhan, Y., Saunders, B. M., Babon, J. J., Kolesnik, T. B., Low, A., Masters, S. L., Willson, T. A., Kedzierski, L., Yao, S., Handman, E., Norton, R. S., and Nicholson, S. E. (2010) *J. Cell Biol.* **190,** 129–141
21. Brenman, J. E., Chao, D. S., Gee, S. H., McGee, A. W., Craven, S. E., Santillano, D. R., Wu, Z., Huang, F., Xia, H., Peters, M. F., Froehner, S. C., and Bredt, D. S. (1996) *Cell* **84,** 757–767
22. Prabhakar, P., Cheng, V., and Michel, T. (2000) *J. Biol. Chem.* **275,** 19416–19421
23. Wang, D., Li, Z., Messing, E. M., and Wu, G. (2005) *J. Biol. Chem.* **280,** 16393–16401
24. Nishiya, T., Kajita, E., Horinouchi, T., Nishimoto, A., and Miwa, S. (2007) *FEBS Lett.* **581,** 3223–3229
25. Nishiya, T., Kajita, E., Miwa, S., and Defranco, A. L. (2005) *J. Biol. Chem.* **280,** 37107–37117
26. Nishiya, T., and DeFranco, A. L. (2004) *J. Biol. Chem.* **279,** 19008–19017
27. Shembade, N., Harhaj, N. S., Parvatiyar, K., Copeland, N. G., Jenkins, N. A., Matesic, L. E., and Harhaj, E. W. (2008) *Nat. Immunol.* **9,** 254–262
28. Ungureanu, D., Saharinen, P., Junttila, I., Hilton, D. J., and Silvennoinen, O. (2002) *Mol. Cell. Biol.* **22,** 3316–3326
29. Gotoh, T., Oyadomari, S., Mori, K., and Mori, M. (2002) *J. Biol. Chem.* **277,** 12343–12350
30. Garvey, E. P., Oplinger, J. A., Furfine, E. S., Kiff, R. J., Laszlo, F., Whittle, B. J., and Knowles, R. G. (1997) *J. Biol. Chem.* **272,** 4959–4963
31. Webb, J. L., Harvey, M. W., Holden, D. W., and Evans, T. J. (2001) *Infect. Immun.* **69,** 6391–6400
32. Vodovotz, Y., Russell, D., Xie, Q. W., Bogdan, C., and Nathan, C. (1995) *J. Immunol.* **154,** 2914–2925
33. Wheeler, M. A., Smith, S. D., García-Cardeña, G., Nathan, C. F., Weiss, R. M., and Sessa, W. C. (1997) *J. Clin. Invest.* **99,** 110–116
34. Sha, Y., Pandit, L., Zeng, S., and Eissa, N. T. (2009) *Mol. Cell. Biol.* **29,** 116–128
35. Filippakopoulos, P., Low, A., Sharpe, T. D., Uppenberg, J., Yao, S., Kuang, Z., Savitsky, P., Lewis, R. S., Nicholson, S. E., Norton, R. S., and Bullock, A. N. (2010) *J. Mol. Biol.* **401,** 389–402
36. Jiang, J., Ballinger, C. A., Wu, Y., Dai, Q., Cyr, D. M., Höhfeld, J., and Patterson, C. (2001) *J. Biol. Chem.* **276,** 42938–42944
37. Chen, L., Kong, X., Fu, J., Xu, Y., Fang, S., Hua, P., Luo, L., and Yin, Z. (2009) *Cell. Immunol.* **258,** 38–43
38. Stuehr, D. J., and Nathan, C. F. (1989) *J. Exp. Med.* **169,** 1543–1555
39. Nathan, C. (1992) *Faseb J.* **6,** 3051–3064
40. Albina, J. E., Cui, S., Mateo, R. B., and Reichner, J. S. (1993) *J. Immunol.* **150,** 5080–5085
41. Sarih, M., Souvannavong, V., and Adam, A. (1993) *Biochem. Biophys. Res. Commun.* **191,** 503–508
42. Messmer, U. K., Lapetina, E. G., and Brüne, B. (1995) *Mol. Pharmacol.* **47,** 757–765
43. Hilbi, H., Zychlinsky, A., and Sansonetti, P. J. (1997) *Parasitology* **115,** (suppl.), S79–S87

AQ: A

Nitric Oxide xxx (2010) xxx–xxx

Contents lists available at ScienceDirect

Nitric Oxide

journal homepage: www.elsevier.com/locate/yniox

Review

Screening systems for the identification of *S*-nitrosylated proteins

Takashi Uehara [a,*], Tadashi Nishiya [b]

[a] *Department of Medicinal Pharmacology, Graduate School of Medicine, Dentistry and Pharmaceutical Sciences, Okayama University, Okayama 700-8530, Japan*
[b] *Department of Cellular Pharmacology, Graduate School of Medicine, Hokkaido University, Sapporo 060-0812, Japan*

ARTICLE INFO

Article history:
Available online xxxx

Keywords:
S-Nitrosylation
Nitric oxide
Screening

ABSTRACT

S-Nitrosylation is a well-characterized reaction involving the covalent binding of nitric oxide (NO) to cysteine residues (Cys) in a protein. Similar to protein phosphorylation, *S*-nitrosylation is a post-translational modification involved in the regulation of a large number of intracellular functions and signaling events. Moreover, like phosphorylation, *S*-nitrosylation is precisely regulated in time and space. A procedure known as the biotin-switch method that specifically detects *S*-nitrosylated proteins (SNO-P) was recently developed by Snyder's group. They found that many proteins are substrates for NO, and several groups have attempted to identify other SNO-P by improving this method. In this review, we describe the SNO-P identified using modified versions of the biotin-switch method.

Contents

Introduction

NO is an important signaling molecule that exerts diverse physiological effects via *S*-nitrosylation, a reversible type of post-translational modification that affects the activity, localization, and stability of proteins [1]. *S*-Nitrosylation involves the oxidation of Cys thiols by NO synthesized by NO synthase (NOS), and by transnitrosylation from low-molecular-weight nitrosothiols such as *S*-nitrosylated Cys or nitrosylated proteins (RSNO) [2–6]. The specificity of *S*-nitrosylation is regulated by several factors, including consensus sequences that increase the chemical reactivity of Cys targets of NO [7], and adaptor proteins near the NOS isoenzymes [8].

To date, a large number of targets of *S*-nitrosylation have been identified and linked to functional consequences. Importantly, protein regulation by *S*-nitrosylation has been coupled to physiological stimuli involving both the receptor-mediated activation of NOS and the stimulus-induced denitrosylation [2,8,9].

S-Nitrosylation (i.e., the covalent attachment of NO to Cys residues) is a post-translational modification that regulates a wide variety of cellular functions and signaling events. Comparable to phosphorylation, *S*-nitrosylation is regulated precisely in time and space [10]. Many reports have demonstrated the dynamic regulation of protein function by reversible modifications; they play a pivotal role in physiological and pathophysiological functions [11]. The characterization of *S*-nitrosylated proteins (SNO-P) and modification sites is an important part of understanding the function of NO in cells. Thus far, several approaches have been developed for the detection of protein *S*-nitrosylation [12]. They can be divided into two categories: direct and indirect. Direct detection methods are considered to be preferable, because they reflect the *in vivo* situation and require minimal sample preparation reducing the possibility of false positives. However, the direct analysis of protein *S*-nitrosylation is difficult because this type of modification is largely unstable and rare. Direct detection by immunoprecipitation or Western blotting is not generally conducted for protein *S*-nitrosylation analysis, because

* Corresponding author. Address: Department of Medicinal Pharmacology, Graduate School of Medicine, Dentistry and Pharmaceutical Sciences, Okayama University, 1-1-1 Tsushima-Naka, Okayama 700-8530, Japan. Fax: +81 86 251 7939.
E-mail address: uehara@pharm.okayama-u.ac.jp (T. Uehara).

1089-8603/$ - see front matter © 2010 Elsevier Inc. All rights reserved.
doi:10.1016/j.niox.2010.11.002

Please cite this article in press as: T. Uehara, T. Nishiya, Screening systems for the identification of *S*-nitrosylated proteins, Nitric Oxide (2010), doi:10.1016/j.niox.2010.11.002

the *S*-nitrosylated (SNO) bond is degraded under the reducing conditions of SDS–PAGE. Antibodies against SNO-P can sometimes produce positive signals by immunohistochemistry [13]. Additionally, the direct identification of *S*-nitrosylation sites by mass spectrometry (MS) is difficult because the SNO bond is very sensitive to UV light [14], and it is labile under conventional collision-induced dissociation conditions [15]. On the other hand, Wang et al. [16] recently identified the *S*-nitrosylation sites on thioredoxin using electrospray ionization (ESI) quadrupole time-of-flight (QTOF) MS. Both sample buffer composition and MS hardware parameters were carefully adjusted to ensure that SNO peptides could be ionized and fragmented with optimal signal/noise ratios. However, the application of this strategy is limited to certain types of instruments, and the adoption of this strategy for the proteome-wide identification of protein *S*-nitrosylation sites in complex protein mixtures remains challenging.

Most other approaches for detecting protein *S*-nitrosylation are indirect, such as measuring free NO levels after cleavage of the SNO bond or conversion of the SNO bond into a detectable tag [12]. For example, chemiluminescence assays have been developed to detect the light released upon the decay of electronically excited nitrogen dioxide (NO_2^-), which is generated by the reaction of free NO released from the SNO bond with ozone [17]. Such methods can effectively determine the total level of protein *S*-nitrosylation present in a biological sample, but they cannot identify specific SNO-P. Fortunately, a number of indirect MS-based proteomics approaches have been developed for the identification of SNO-P and their modification sites from complex biological samples [18,19].

The biotin-switch technique, an epoch-making SNO-P detection method

Proteins that are susceptible to *S*-nitrosylation are difficult to identify due to the lack of an effective detection method and the development of such a method is complicated by the unstable oxidation states of the proteins involved. However, the development of the biotin-switch method by Jeffrey and Snyder for the detection of SNO-P enabled researchers to overcome this problem by exchanging the labile RSNO modification for a readily detectable biotin tag [20]. This method has facilitated the large-scale detection of cellular SNO substrates [18,20] (Fig. 1).

The biotin-switch method consists of three steps: the methylthiolation of free Cys thiols with methyl methanethiosulfonate (MMTS), the reduction of SNO bonds to thiols with ascorbate, and the ligation of the nascent thiols with *N*-[6-(biotinamido)hexyl]-3′-(2′-pyridyldi thio)-propionamide (biotin-HPDP). In combination with MS, several potential SNO-P have been discovered in *Homosapiens*, *Mus musculus*, and *Arabidopsis thaliana* [21–24] (Fig. 1). However, it needs pay attention to the results performed by this method, since there might be some cases where (1) ascorbate-induced reduction of SNO bonds to thiols is not complete, and (2) other modifications ("soft" disulfides or sulfenic acid) could also be reduced to thiol. In addition, NO sometimes leaves from the protein due to destabilization when protein secondary/tertiary structure is lost with SDS. Therefore, additional possible candidates might be identified by using other reagents instead of SDS.

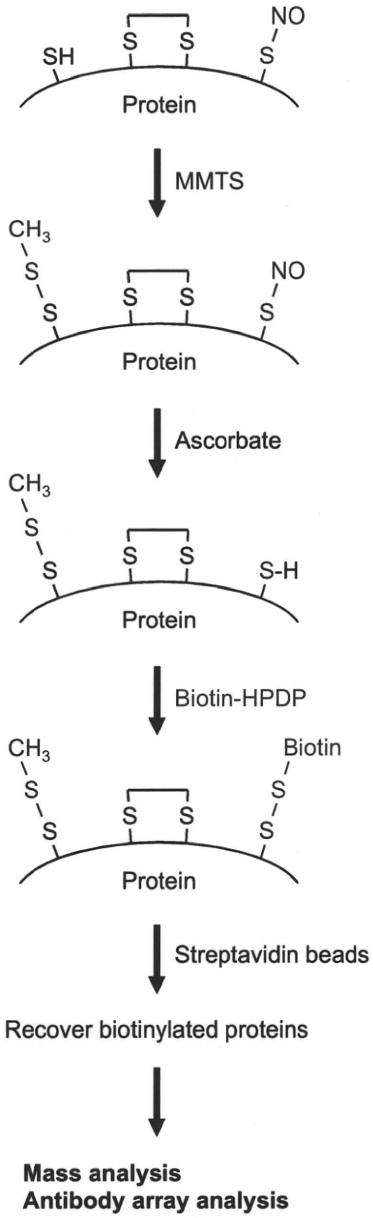

Fig. 1. Schematic representation for detecting *S*-nitrosylated proteins. Free thiols are blocked by methylthiolation reagent with MMTS. Then, nitrosothiols are specifically reduced with ascorbate to change the thiols. Finally, newly reformed cysteines are reacted with thiol-modifying reagent biotin-HPDP and detected with several protocols.

Identification of SNO-P by MS

The biotin-switch method is commonly used to detect endogenous SNO-P, and has greatly advanced the field [18,20]; however, numerous other methods have been developed for the detection of SNO-P. Gross and co-workers [19,25] developed a method for the application of an unbiased proteome that was recently shown to identify predominant *S*-nitrosylation sites on Cys residues in complex protein mixtures. This method, termed SNOSID, allows for proteome-wide *S*-nitrosylation site identification. They extended the capability of the biotin-switch method by introducing a proteolytic digestion step before avidin capture, which allows for the selective isolation of peptides that previously contained SNO Cys residues. In total, 68 SNO peptides from 56 rat cerebellar proteins were identified in this way (Fig. 2).

On the other hand, Camerini et al. [26] used an N-terminally modified His tag to selectively label and detect nitrosylated peptides. However, the number of SNO-Ps detected was relatively low, presumably due to the relatively large mass shift introduced by the tag. A large tag seems to prevent the identification of large peptides due to the limited mass detection window (Fig. 2).

A two-dimensional differential gel electrophoresis approach has also been applied for the visualization of SNO-P. However, few SNO-P have been identified using this method due to their low

Please cite this article in press as: T. Uehara, T. Nishiya, Screening systems for the identification of *S*-nitrosylated proteins, Nitric Oxide (2010), doi:10.1016/j.niox.2010.11.002

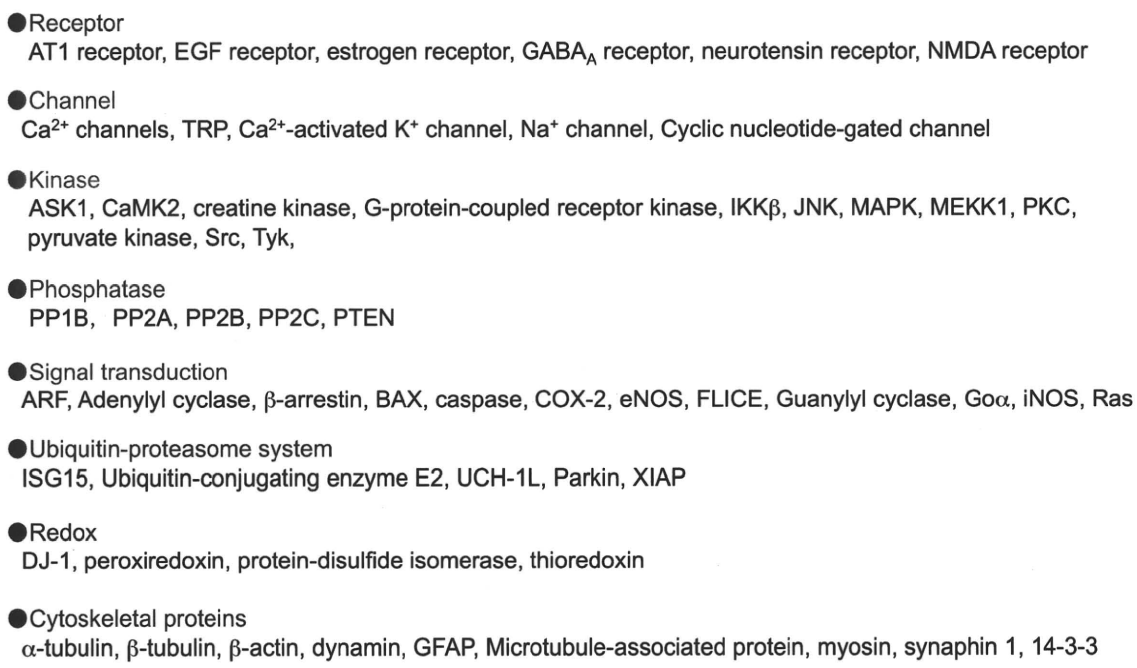

Fig. 2. Typical *S*-nitrosylated proteins. In this figure, the known *S*-nitrosylated proteins are classified into each function indicated. AT, angiotensin; EGF, epidermal growth factor; GABA, γ-aminobutyric acid; NMDA, *N*-methyl-D-aspartic acid; TRP, transient receptor potential; ASK, apoptosis signal-regulating kinase; CaMK, calcium/calmodulin-dependent protein kinase; IKK, IκB kinase; JNK, Jun N-terminal kinase; MAPK, mitogen-activated protein kinase; MEKK, mitogen-activated protein kinase/extracellular signal-regulated kinase kinase kinase; PP, protein phosphatase; PTEN, phosphatase and tensin homolog; ARF, ADP ribosylation factor; Bax, BCL2-associated X protein; COX, cyclooxygenase; FLICE, FADD-like interleukin-1 beta-converting enzyme; ISG, interferon stimulated gene; UCH, ubiquitin carboxyl-terminal esterase L1; XIAP, X-linked inhibitor of apoptosis protein; GFAP, glial fibrillary acidic protein.

abundance and the low recovery of SNO peptides from in-gel digestion [12].

Recently, a resin-assisted capture (RAC)-based method was developed to isolate SNO-P. This method combines the "labeling" and "pull-down" steps from the biotin-switch method into a single step [27,28]. Using this approach, Forrester et al. [27] reported the identification of 47 and 44 *S*-nitrosylation sites from RAW264.7 macrophages and *Escherichia coli*, respectively. However, neither the biotin-switch method nor the RAC-based approach was effective for *S*-nitrosylation site identification. Additionally, to identify stable protein nitrosothiols, a proteomic method for profiling *S*-nitrosylation was examined. They developed a quantitative nitroso-proteomic approach for the screening of dozens of known and unknown SNO-P, and succeeded in finding a novel class of target proteins that were capable of forming stable nitrosothiols (Fig. 2).

Identification of SNO-P by protein arrays

As described above, the biotin-switch method, which converts an *S*-nitrosothiol into an *S*-biotinylated Cys, has greatly facilitated the identification of SNO-P and the specific SNO sites and aided in the discovery of many new physiological or pathophysiological roles for *S*-nitrosylation. The characterization of SNO proteomes using a protein array has revealed several classes of *S*-nitrosylation-reactive proteins. Microarray-based proteomic screens of *S*-nitrosylation may reveal SNO-reactivity patterns for large classes of proteins. Foster et al. [29] attempted to use a protein microarray-based approach to investigate the determinants of *S*-nitrosylation in biologically relevant low-mass *S*-nitrosothiols. They identified large sets of yeast and human target proteins, among which those with active-site Cys thiols residing at the N termini of α-helices or within catalytic loops were particularly prominent (Fig. 2). Interestingly, structural motifs such as a Cys at the N terminus of a helix were highly variable with regard to *S*-nitrosylation-reactivity, and are, therefore, unlikely to be universal motifs for *S*-nitrosylation.

Identification of SNO-P by computer analysis

Computational studies of post-translational modifications are very attractive because more than 150 databases and computational tools have been developed for such analyses. In fact, several approaches have been used to find the *S*-nitrosylation sites in proteins. Xue et al. [30] developed an algorithm GPS 2.0 (Group-based prediction system) for the prediction of kinase-specific phosphorylation sites. They further reported substantial improvement of the method and the release of GPS 3.0 algorithm, and they developed the novel computational software of GPS-SNO 1.0 for the prediction of *S*-nitrosylation sites [31]. Leave-one-out and 4-, 6-, 8-, and 10-fold cross validations were calculated to evaluate the prediction performance and system robustness. By comparison, the performance of the GPS 3.0 algorithm was better than that of several other approaches, with an accuracy of 75.80%, a sensitivity of 53.57%, and a specificity of 80.14% under low-threshold conditions. These proteins were detected from large- or small-scale studies, and the exact *S*-nitrosylation sites had not been experimentally determined. They proposed that GPS-SNO 1.0 is a useful tool for the identification of potential *S*-nitrosylation sites (Fig. 2).

References

[1] T. Hess, A. Matsumoto, S.O. Kim, H.E. Marshall, J.S. Stamler, Protein *S*-nitrosylation: purview and parameters, Nat. Rev. Mol. Cell Biol. 6 (2005) 150–166.
[2] K. Inoue, T. Akaike, Y. Miyamoto, T. Okamoto, T. Sawa, M. Otagiri, S. Suzuki, T. Yoshimura, H. Maeda, Nitrosothiol formation catalyzed by ceruloplasmin: implication for cytoprotective mechanism in vivo, J. Biol. Chem. 274 (1999) 27069–27075.
[3] J.S. Stamler, G. Meissner, Physiology of nitric oxide in skeletal muscle, Physiol. Rev. 81 (2001) 209–237.

Please cite this article in press as: T. Uehara, T. Nishiya, Screening systems for the identification of *S*-nitrosylated proteins, Nitric Oxide (2010), doi:10.1016/j.niox.2010.11.002

[4] J.R. Pawloski, D.T. Hess, J.S. Stamler, Export by red blood cells of nitric oxide bioactivity, Nature 409 (2001) 622–626.
[5] M.W. Foster, T.J. McMahon, J.S. Stamler, S-Nitrosylation in health and disease, Trends Mol. Med. 9 (2003) 160–168.
[6] D.A. Mitchell, M.A. Marletta, Thioredoxin catalyzes the S-nitrosylation of the caspase-3 active site cysteine, Nat. Chem. Biol. 1 (2005) 154–158.
[7] J.S. Stamler, E.J. Toone, S.A. Lipton, N.J. Sucher, (S)NO signals: translocation, regulation, and a consensus motif, Neuron 18 (1997) 691–696.
[8] J.S. Paige, S.R. Jaffrey, Pharmacologic manipulation of nitric oxide signaling: targeting NOS dimerization and protein–protein interactions, Curr. Top. Med. Chem. 7 (2007) 97–114.
[9] M. Benhar, M.T. Forrester, D.T. Hess, J.S. Stamler, Regulated protein denitrosylation by cytosolic and mitochondrial thioredoxins, Science 320 (2008) 1050–1054.
[10] M.C. Broillet, S-Nitrosylation of proteins, Cell. Mol. Life Sci. 55 (1999) 1036–1042.
[11] J.S. Stamler, S. Lamas, F.C. Fang, Nitrosylation: the prototypic redox-based signaling mechanism, Cell 106 (2001) 675–683.
[12] F. Torta, V. Usuelli, A. Malgaroli, A. Bachi, Proteomic analysis of protein S-nitrosylation, Proteomics 8 (2008) 4484–4494.
[13] Y. Iwakiri, A. Satoh, S. Chatterjee, D.K. Toomre, C.M. Chalouni, D. Fulton, R.J. Groszmann, V.H. Shah, W.C. Sessa, Nitric oxide synthase generates nitric oxide locally to regulate compartmentalized protein S-nitrosylation and protein trafficking, Proc. Natl. Acad. Sci. USA 103 (2006) 19777–19782.
[14] H.S. Park, S.H. Huh, M.S. Kim, S.H. Lee, E.J. Choi, Nitric oxide negatively regulates c-Jun N-terminal kinase/stress-activated protein kinase by means of S-nitrosylation, Proc. Natl. Acad. Sci. USA 97 (2000) 14382–14387.
[15] G. Hao, S.S. Gross, Electrospray tandem mass spectrometry analysis of S- and N-nitrosopeptides: facile loss of NO and radical-induced fragmentation, J. Am. Soc. Mass Spectrom. 17 (2006) 1725–1730.
[16] Y. Wang, T. Liu, C. Wu, H. Li, A strategy for direct identification of protein S-nitrosylation sites by quadrupole time-of-flight mass spectrometry, J. Am. Soc. Mass Spectrom. 19 (2008) 1353–1360.
[17] A. Gow, A. Doctor, J. Mannick, B. Gaston, S-Nitrosothiol measurements in biological systems, J. Chromatogr. 851 (2007) 140–151.
[18] S.R. Jaffrey, S.H. Snyder, The biotin switch method for the detection of S-nitrosylated proteins, Sci. STKE 2001 (2001) pl1.
[19] G. Hao, B. Derakhshan, L. Shi, F. Campagne, S.S. Gross, SNOSID, a proteomic method for identification of cysteine S-nitrosylation sites in complex protein mixtures, Proc. Natl. Acad. Sci. USA 103 (2006) 1012–1017.
[20] S.R. Jaffrey, H. Erdjument-Bromage, C.D. Ferris, P. Tempst, S.H. Snyder, Protein S-nitrosylation: a physiological signal for neuronal nitric oxide, Nat. Cell Biol. 3 (2001) 193–197.
[21] L. Lefièvre, Y. Chen, S.J. Conner, J.L. Scott, S.J. Publicover, W.C. Ford, C.L. Barratt, Human spermatozoa contain multiple targets for protein S-nitrosylation: an alternative mechanism of the modulation of sperm function by nitric oxide? Proteomics 7 (2007) 3066–3084.
[22] B. Huang, S.C. Chen, D.L. Wang, Shear flow increases S-nitrosylation of proteins in endothelial cells, Cardiovasc. Res. 83 (2009) 536–546.
[23] T. Kuncewicz, E.A. Sheta, I.L. Goldknopf, B.C. Kone, Proteomic analysis of S-nitrosylated proteins in mesangial cells, Mol. Cell. Proteomics 2 (2003) 156–163.
[24] C. Lindermayr, G. Saalbach, J. Durner, Proteomic identification of S-nitrosylated proteins in Arabidopsis, Plant Physiol. 137 (2005) 921–930.
[25] B. Derakhshan, P.C. Wille, S.S. Gross, Unbiased identification of cysteine S-nitrosylation sites on proteins, Nat. Protoc. 2 (2007) 1685–1691.
[26] S. Camerini, M.L. Polci, U. Restuccia, V. Usuelli, A. Malgaroli, A. Bachi, A novel approach to identify proteins modified by nitric oxide: the HIS-TAG switch method, J. Proteome Res. 6 (2007) 3224–3231.
[27] M.T. Forrester, J.W. Thompson, M.W. Foster, L. Nogueira, M.A. Moseley, J.S. Stamler, Proteomic analysis of S-nitrosylation and denitrosylation by resin-assisted capture, Nat. Biotechnol. 27 (2009) 557–559.
[28] M.W. Forrester, D.T. Hess, J.W. Thompson, R.C. Hultman, M.A. Moseley, J.S. Stamler, P.J. Casey, Site-specific analysis of protein S-acylation by resin-assisted capture (Acyl-RAC), J. Lipid. Res., in press.
[29] M.W. Foster, M.T. Forrester, J.S. Stamler, A protein microarray-based analysis of S-nitrosylation, Proc. Natl. Acad. Sci. USA 106 (2009) 18948–18953.
[30] Y. Xue, J. Ren, X. Gao, C. Jin, L. Wen, X. Yao, GPS 2.0, a tool to predict kinase-specific phosphorylation sites in hierarchy, Mol. Cell. Proteomics 7 (2008) 1598–1608.
[31] Y. Xue, Z. Liu, X. Gao, C. Jin, L. Wen, Y. Yao, J. Ren, GPS-SNO: computational prediction of protein S-nitrosylation sites with a modified GPS algorithm, PLoS ONE 5 (2010) e11290.

Please cite this article in press as: T. Uehara, T. Nishiya, Screening systems for the identification of S-nitrosylated proteins, Nitric Oxide (2010), doi:10.1016/j.niox.2010.11.002

J Pharmacol Sci 113, 276 – 280 (2010)

Journal of Pharmacological Sciences

Short Communication

Endothelin Type B Receptor–Induced Sustained Ca^{2+} Influx Involves $G_{q/11}$/Phospholipase C–Independent, p38 Mitogen-Activated Protein Kinase–Dependent Activation of Na^+/H^+ Exchanger

Tsunaki Higa[1,†], Takahiro Horinouchi[1,†], Hiroyuki Aoyagi[1], Hiroshi Asano[1], Tadashi Nishiya[1], Arata Nishimoto[1], Ikunobu Muramatsu[2], and Soichi Miwa[1,*]

[1]*Department of Cellular Pharmacology, Hokkaido University Graduate School of Medicine, Sapporo 060-8638, Japan*
[2]*Division of Pharmacology, Department of Biochemistry and Bioinformative Sciences, School of Medicine, University of Fukui, Fukui 910-1193, Japan*

Received April 12, 2010; Accepted May 14, 2010

Abstract. The mechanism for sustained Ca^{2+} influx activated by G protein–coupled receptors was examined. In Chinese hamster ovary cells expressing recombinant human endothelin type B receptor (ET_BR) and endogenous P2Y receptor (P2Y-R), endothelin-1 elicited a sustained Ca^{2+} influx depending on $G_{q/11}$ protein, phospholipase C (PLC), Na^+/H^+ exchanger (NHE), and p38 mitogen-activated protein kinase (p38MAPK), whereas P2Y-R–induced sustained Ca^{2+} influx was negligible. Functional studies showed that NHE activation by ET_BR was mediated via p38MAPK but not $G_{q/11}$/PLC, while that by P2Y-R involves only $G_{q/11}$/PLC/p38MAPK. These results suggest that $G_{q/11}$/PLC-independent NHE activation via p38MAPK plays an important role in ET_BR-mediated sustained Ca^{2+} influx.

Keywords: endothelin type B receptor, Na^+/H^+ exchanger, p38 mitogen-activated protein kinase

G protein–coupled receptors (GPCRs) including endothelin type A receptor (ET_AR) and ET_BR transduce the binding of their agonists into activation of G protein–regulated effectors and changes in levels of corresponding second messengers. It is well-known that stimulation of G_q protein–coupled receptors induces formation of second messengers such as inositol 1,4,5-trisphosphate (IP_3) and diacylglycerol (DAG) via phospholipase C (PLC). Binding of IP_3 to its receptor on the endoplasmic reticulum (ER) triggers Ca^{2+} release from the ER, resulting in a transient increase in intracellular free Ca^{2+} concentration ($[Ca^{2+}]_i$) (1). According to the classical theory, this is followed by a sustained increase in $[Ca^{2+}]_i$, resulting from Ca^{2+} influx through several types of voltage-independent Ca^{2+}-permeable cation channels such as store-operated Ca^{2+} channels (SOCCs) (2). On the other hand, DAG directly activates receptor-operated Ca^{2+} channels (ROCCs), leading to sustained Ca^{2+} influx. Thus, the sustained increase in $[Ca^{2+}]_i$ via SOCCs and ROCCs results from activation of the $G_{q/11}$/PLC pathway.

Recently, we have reported that in addition to Ca^{2+} influx through SOCC and ROCC activated via $G_{q/11}$/PLC (3, 4), ET_AR induced $G_{q/11}$/PLC-independent activation of sustained Ca^{2+} influx that is not mediated through either SOCC or ROCC: the Ca^{2+} influx is mediated by the reverse mode of the Na^+/Ca^{2+} exchanger functionally coupled with Na^+/H^+ exchanger (NHE) via Na^+ transport (5). Furthermore, NHE activation in response to ET_AR stimulation is mediated via p38 mitogen–activated protein kinase (p38MAPK), which is activated through G_{12} protein (6). Because $G_{q/11}$-coupled receptors can couple to other G proteins, these findings imply that mechanisms for sustained Ca^{2+} influx might be different depending on the type of GPCRs to be activated.

In the present study, in order to expand the functional significance of $G_{q/11}$/PLC-independent, p38MAPK-dependent NHE activation in sustained Ca^{2+} influx to other GPCRs coupled with $G_{q/11}$/PLC and $G_{12/13}$, we examined whether this mechanism is involved in the Ca^{2+} influx induced by recombinant ET_BR and endogenous P2Y re-

†These authors contributed equally to this work.
*Corresponding author. smiwa@med.hokudai.ac.jp
Published online in J-STAGE on June 29, 2010 (in advance)
doi: 10.1254/jphs.10102SC

ceptor (P2Y-R) expressed in CHO cells (7).

To generate CHO cells stably expressing ET_BR (ET_BR-CHO), the gene of human ET_BR fused with yellow fluorescence protein at the C terminus was introduced into CHO cells by retroviral gene transfer as previously described (5, 6). $[Ca^{2+}]_i$ was monitored by using fluorescent Ca^{2+} indicators, fura-2/acetoxymethyl ester (fura-2/AM) and fluo-3/AM (5, 6). To determine molecular mechanisms for NHE activation upon stimulation of ET_BR and P2Y-R with ET-1 and adenosine triphosphate (ATP), respectively, the change in extracellular acidification rate (ECAR) was measured by the eight-channel Cytosensor™ microphysiometer (Molecular Devices Corp., Sunnyvale, CA, USA) (5, 6). To estimate the degree of p38MAPK activation after stimulation of ET_BR and P2Y-R, the phosphorylation levels of p38MAPK were estimated by Western blot analysis (6).

The concentration–response curves for ET-1 and ATP were constructed to evaluate its EC_{50} value (M) using GraphPad PRISM™ (version 3.00; GraphPad Software Inc., San Diego, CA, USA). The EC_{50} values were converted to negative logarithmic values (pEC_{50}) for analysis. Results of Cytosensor™ microphysiometer studies are expressed as percentages of the basal ECAR prior to exposure to vehicle or inhibitors. All data were presented as means ± S.E.M., where n refers to the number of experiments. The significance of the difference between mean values was evaluated with GraphPad PRISM™ by Student's paired *t*-test or one-way analysis of variance (ANOVA) followed by Tukey's multiple comparison test. A *P* value less than 0.05 was considered to indicate significant differences.

In ET_BR-CHO, stimulation of ET_BR with 1 nM ET-1 elicited a biphasic increase in $[Ca^{2+}]_i$ consisting of an initial transient peak (304.9 ± 31.6 nM, n = 5) and a subsequent sustained increase (199.8 ± 16.0 nM, n = 5). The pEC_{50} values for ET-1–induced increase in $[Ca^{2+}]_i$ were 10.09 ± 0.13 for the transient phase and 9.72 ± 0.18 for the sustained phase (Fig. 1: A and B). ATP also induced a transient increase in $[Ca^{2+}]_i$ with a pEC_{50} value of 5.86 ± 0.08 and the maximum increase in $[Ca^{2+}]_i$ of 386.4 ± 39.5 nM (n = 5). ATP can activate two families of P2 receptors, the ligand-gated ion channels (P2X-R) (8) and the G protein–coupled P2Y-R (7), which are endogenously expressed in CHO cells. ATP-induced increase in $[Ca^{2+}]_i$ seems to be mediated via P2Y-R but not P2X-R, since the Ca^{2+} response was completely inhibited by 1 μM YM-254890, a $G_{q/11}$ inhibitor (data not shown). Notably, the sustained increase in $[Ca^{2+}]_i$ was very small for each of the tested concentrations of ATP (Fig. 1B). Interestingly, although the transient $[Ca^{2+}]_i$ increases induced by 1 nM ET-1 and by 10 μM ATP in ET_BR-CHO are comparable with each other (Fig. 1A), there is a marked difference in the amplitude of the sustained Ca^{2+} responses. These results suggest that store depletion does not necessarily activate SOCCs and hence that the ET_BR-induced sustained Ca^{2+} influx is not due to SOCCs activated by the emptying of the intracellular Ca^{2+} store.

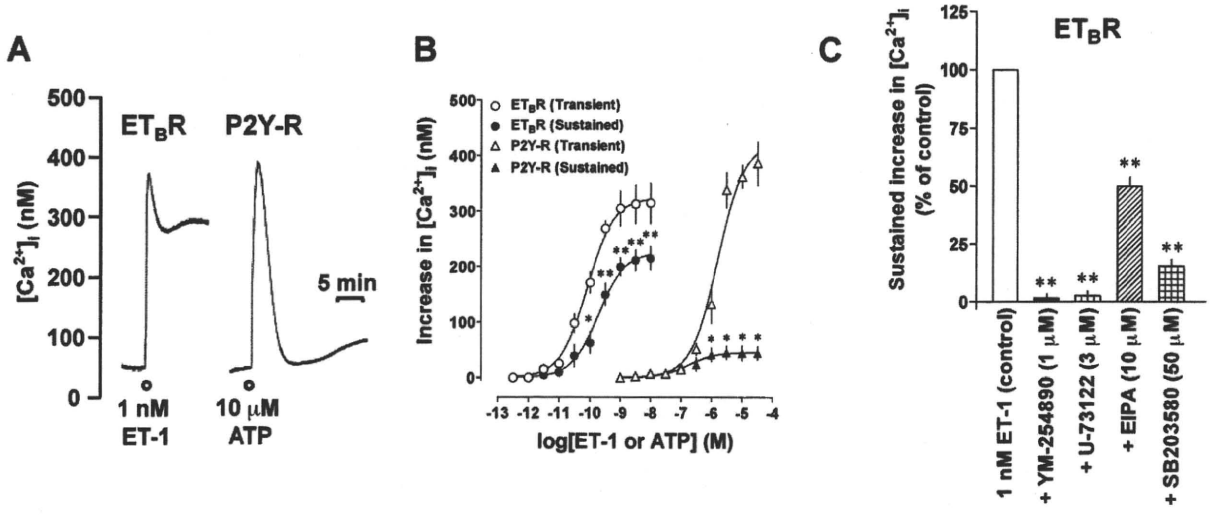

Fig. 1. Characterization of the increases in $[Ca^{2+}]_i$ induced by ET-1 and ATP in ET_BR-CHO. A) Representative traces showing the $[Ca^{2+}]_i$ increases induced by stimulation of ET_BR with ET-1 and of P2Y-R with ATP at indicated concentrations. B) Concentration–response curves for the transient and sustained $[Ca^{2+}]_i$ increases triggered by ET-1 and ATP. The sustained $[Ca^{2+}]_i$ increases were measured 10 and 20 min after addition of ET-1 and ATP, respectively. $^*P < 0.05$, $^{**}P < 0.01$, sustained $[Ca^{2+}]_i$ increases induced by these agonists vs. basal Ca^{2+} level. C) Effects of YM-254890, U-73122, EIPA, and SB203580 on the 1 nM ET-1–induced sustained increases in $[Ca^{2+}]_i$. Data are presented as means ± S.E.M. of the results obtained from 5 experiments. $^{**}P < 0.01$, vs. its control (1 nM ET-1 alone, open column).

To determine the signaling molecules involving sustained Ca^{2+} influx induced by ET-1, a specific inhibitor was added during the sustained phase of $[Ca^{2+}]_i$ increase. Maximally effective concentrations of a $G_{q/11}$ inhibitor (1 μM YM-254890), a PLC inhibitor (3 μM U-73122), an NHE inhibitor [10 μM 5-(*N*-ethyl-*N*-isopropyl)amiloride, EIPA], and a p38MAPK inhibitor (50 μM SB203580) inhibited the ET-1–induced sustained increases, indicating that the sustained Ca^{2+} responses to ET-1 are mediated via $G_{q/11}$, PLC, NHE, and p38MAPK. This result in turn implies that like ET_AR (6), an NHE/p38MAPK-dependent mechanism is involved in the ET_BR-induced sustained Ca^{2+} influx.

Recently, we have shown that a $G_{q/11}$/PLC-independent, p38MAPK-dependent pathway regulates NHE activity after ET_AR stimulation (6). To clarify intracellular mechanisms responsible for NHE activation by ET_BR, we used the Cytosensor™ microphysiometer, a valuable tool for evaluating NHE function in living cells (5, 6). Functional study with this instrument showed that 1 nM ET-1 and 10 μM ATP evoked an increase in ECAR. The increases by ATP were far smaller than those by ET-1 (e.g., 124.9% for ATP vs. 162.2% for ET-1 at 6 min) (Fig. 2). The responses to ET-1 and ATP were markedly inhibited by 10 μM EIPA, indicating the involvement of NHE. To identify upstream signaling molecules in NHE activation by ET_BR and P2Y-R, the effects of YM-254890, U-73122, and SB203580 on the ECAR response were examined. In contrast to the Ca^{2+} response, the ECAR response was resistant to both YM-254890 and U-73122, but sensitive to SB203580 (Fig. 2A). On the other hand, the ATP-induced increase in ECAR was sensitive to all of these inhibitors (Fig. 2B). These findings suggest that activation of NHE is mediated via a $G_{q/11}$/PLC-independent, p38MAPK-dependent pathway for ET_BR and via a $G_{q/11}$/PLC/p38MAPK-dependent pathway for P2Y-R.

Increasing evidence indicates that p38MAPK plays an important role in both activation of NHE by GPCRs (9, 10) and sustained Ca^{2+} response induced by ET_AR (5, 6). In addition, activation of p38MAPK by ET_AR is reported to be independent of the $G_{q/11}$/PLC pathway (6). To examine the role of p38MAPK activation in the signaling for ET_BR and P2Y-R, p38MAPK phosphorylation was measured by western blot analysis. The p38MAPK phosphorylation by 1 nM ET-1 was exceedingly strong and persistent, whereas that by 10 μM ATP was very weak and transient (Fig. 3A). At 15 min following stimulation, ET-1 induced a concentration-dependent phosphorylation of p38MAPK with a pEC_{50} value of 10.28 ± 0.12 and the maximum level of 879.9 ± 52.2% (n = 6, Fig. 3B), but ATP (1 – 30 μM) induced no significant increase. To determine upstream regulatory molecules for p38MAPK, the effects of inhibitors for $G_{q/11}$ and PLC on the ET-1–induced p38MAPK phosphorylation were examined. Like p38MAPK activation via ET_AR (6), YM-254890 (1 μM) and U-73122 (10 μM) had little effect on p38MAPK phosphorylation by 1 nM ET-1 (data not shown). Taken together with the above-mentioned Cytosensor™ microphysiometer study, these data provide further evidence for the involvement of the $G_{q/11}$/PLC-independent pathway in ET_BR-induced p38MAPK activation. We were unable to determine the upstream molecules for ATP-induced p38MAPK phosphorylation because its phosphorylation level was too weak to analyze.

Like ET_AR, both ET_BR and P2Y-R can couple with a member of the G_{12} family (G_{12} and G_{13} proteins) in addition to $G_{q/11}$ protein (11 – 13), and activation of G_{12} protein is involved in ET_AR-induced NHE activation via p38MAPK, causing a sustained increase in $[Ca^{2+}]_i$ (6). Interestingly, G_{13} protein is a potential candidate responsible for NHE activation mediated via ET_BR (13), despite stimulation of GPCRs coupled to G_q (10) and $G_{12/13}$ (14)

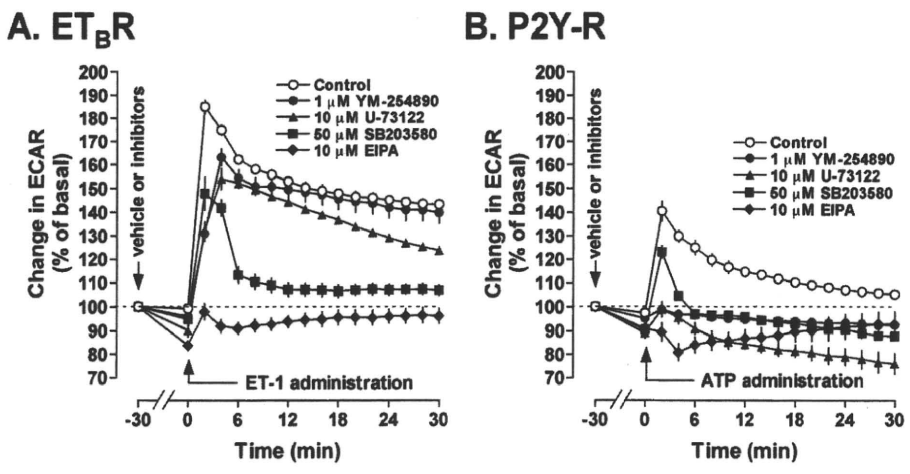

Fig. 2. Characterization of changes in ECAR induced by 1 nM ET-1 (A) and 10 μM ATP (B) in ET_BR-CHO. The change in ECAR was measured by the Cytosensor™ microphysiometer every 2 min. The cells were treated with either vehicle (0.2% dimethylsulfoxide) or inhibitors for 30 min before stimulation with ET-1 (ET-1 administration) or ATP (ATP administration) for 30 min. Data are presented as means ± S.E.M. of the results obtained from 5 experiments.

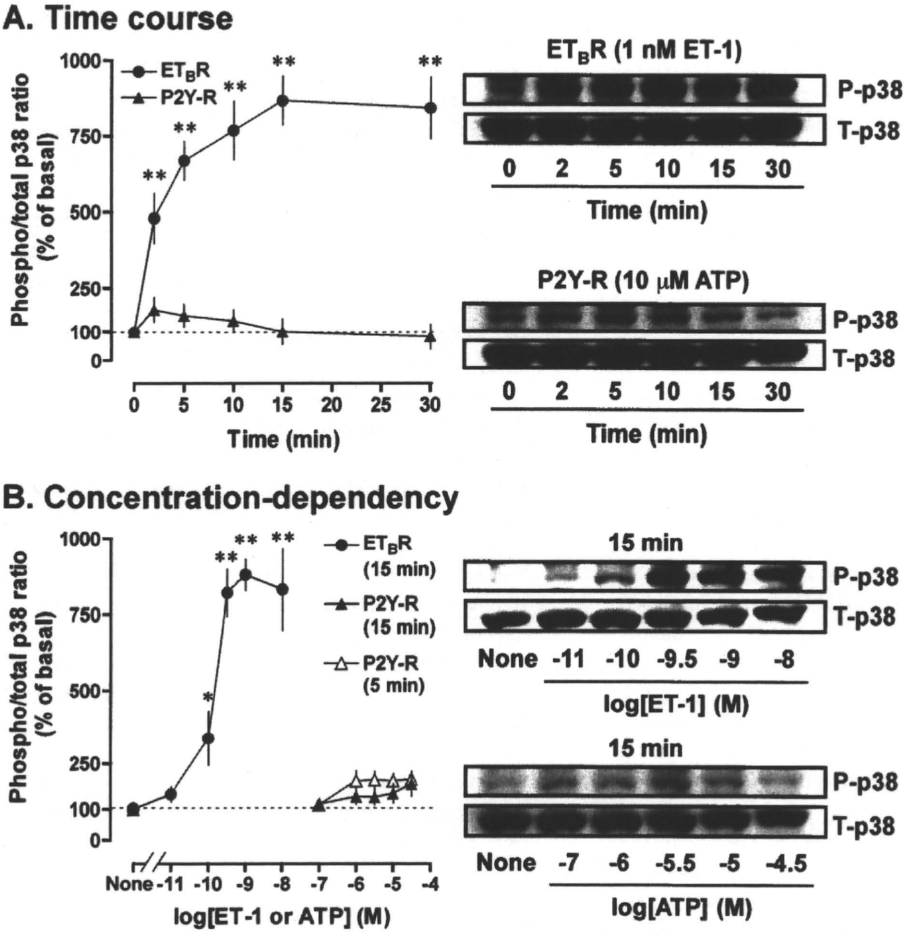

Fig. 3. Characterization of p38MAPK phosphorylation in response to ET-1 and ATP in ET_BR-CHO. A) The time course of p38MAPK phosphorylation induced by 1 nM ET-1 and 10 μM ATP with, at the right, representative immunoblots (P-p38, phosphorylated p38MAPK; T-p38, total p38MAPK). B) Concentration–response curves for p38MAPK phosphorylation in response to 15-min exposure to ET-1 and 5- or 15-min exposure to ATP, with, at the right, representative immunoblots. Data are presented as means ± S.E.M. of the results obtained from 6 experiments. $^*P < 0.05$, $^{**}P < 0.01$, p38MAPK phosphorylation induced by these agonists vs. basal p38MAPK phosphorylation level.

being able to activate NHE. In analogy with the case of ET_AR (6), the EIPA-sensitive part of the ET_BR-induced sustained increase in $[Ca^{2+}]_i$ is mediated by NHE, which is in turn activated via p38MAPK: the remaining part of the $[Ca^{2+}]_i$ increase that is resistant to EIPA is considered to be mediated through ROCCs and/or SOCCs, whose activation requires both $G_{q/11}$/PLC and p38MAPK. An activator of p38MAPK may be $G_{12/13}$ protein. In contrast, the minimum level of the sustained increase in $[Ca^{2+}]_i$ following stimulation of P2Y-R seems to be due to a low level of p38MAPK activation, causing weak activation of NHE and also ROCCs/SOCCs. The low level of p38MAPK activation might be weak coupling of P2Y-R with $G_{12/13}$ protein. Further studies will be required to confirm the possible involvement of G_{12} and/or G_{13} proteins in ET_BR-mediated p38MAPK activation. In addition, the reasons for these differences in signaling cascade and sustained Ca^{2+} response between ET_BR and P2Y-R are not known, but such phenomena may result from the difference in receptor expression level that affects receptor–G-protein coupling in recombinant expression systems (9, 15). Recently, we showed that a difference in expression level of human ET_AR results in a multiplicity of receptor signaling as follows: the ECAR response to ET-1 in low-expressor clone is mediated via the $G_{q/11}$/PLC/p38MAPK/NHE pathway, while the response in high-expressor clone is mediated via either $G_{q/11}$/PLC/NHE or non-$G_{q/11}$(G_{12})/p38MAPK/NHE cascades (6). The signaling cascades for low- and high-expressor are consistent with those utilized by P2Y-R and ET_BR, respectively. Therefore, there is the possibility that the difference in intracellular signaling mechanism between ET_BR and P2Y-R are due to differences in their expression levels and/or the difference of receptor type.

In summary, the present study demonstrated that $G_{q/11}$/PLC-independent activation of NHE via p38MAPK is involved in a sustained increase in $[Ca^{2+}]_i$ triggered by ET_BR but not P2Y-R. Taken together with our previous reports indicating the participation of G_{12}/p38MAPK/NHE cascade in the ET_AR-mediated sustained $[Ca^{2+}]_i$ increase (6), these results imply that $G_{q/11}$/PLC-independent, p38MAPK-dependent activation of NHE plays an important role in the sustained Ca^{2+} response to stimulation of ET_BR in addition to ET_AR.

Acknowledgments

We thank Astellas Pharma Inc. (Tokyo) for the generously providing YM-254890. This study was supported in part by Grant-in-Aids for Young Scientific Research (B) from the Ministry of Education, Culture, Sports, Science, and Technology (MEXT), Japan (T.H.) and for Scientific Research (B) from Japan Society for the Promotion of Science (JSPS) (S.M.) and by grants from Smoking Research Foundation of Japan (S.M.), The Shimabara Science Promotion Foundation (T.H.), and Actelion Pharmaceuticals Japan, Ltd. (T.H.).

References

1 Berridge MJ, Bootman MD, Roderick HL. Calcium signalling: dynamics, homeostasis and remodelling. Nat Rev Mol Cell Biol. 2003;4:517–529.

2 Spassova MA, Soboloff J, He LP, Hewavitharana T, Xu W, Venkatachalam K, et al. Calcium entry mediated by SOCs and TRP channels: variations and enigma. Biochim Biophys Acta. 2004;1742:9–20.

3 Miwa S, Kawanabe Y, Okamoto Y, Masaki T. Ca^{2+} entry channels involved in endothelin-1-induced contractions of vascular smooth muscle cells. J Smooth Muscle Res. 2005;41:61–75.

4 Kawanabe Y, Okamoto Y, Miwa S, Hashimoto N, Masaki T. Molecular mechanisms for the activation of voltage-independent Ca^{2+} channels by endothelin-1 in Chinese hamster ovary cells stably expressing human $endothelin_A$ receptors. Mol Pharmacol. 2002;62:75–80.

5 Horinouchi T, Miyake Y, Nishiya T, Nishimoto A, Morishima S, Muramatsu I, et al. Functional role of Na^+/H^+ exchanger in Ca^{2+} influx mediated via human endothelin type A receptor stably expressed in Chinese hamster ovary cells. J Pharmacol Sci. 2008; 107:456–459.

6 Horinouchi T, Asano H, Higa T, Nishimoto A, Nishiya T, Muramatsu I, et al. Differential coupling of human endothelin type A receptor to $G_{q/11}$ and G_{12} proteins: the functional significance of receptor expression level in generating multiple receptor signaling. J Pharmacol Sci. 2009;111:338–351.

7 Dickenson JM, Blank JL, Hill SJ. Human adenosine A1 receptor and $P2Y_2$-purinoceptor-mediated activation of the mitogen-activated protein kinase cascade in transfected CHO cells. Br J Pharmacol. 1998;124:1491–1499.

8 Michel AD, Chessell IP, Hibell AD, Simon J, Humphrey PP. Identification and characterization of an endogenous $P2X_7$ (P2Z) receptor in CHO-K1 cells. Br J Pharmacol. 1998;125:1194–1201.

9 Sato M, Horinouchi T, Hutchinson DS, Evans BA, Summers RJ. Ligand-directed signaling at the β_3-adrenoceptor produced by 3-(2-ethylphenoxy)-1-[(1,S)-1,2,3,4-tetrahydronapth-1-ylamino]-2S-2-propanol oxalate (SR59230A) relative to receptor agonists. Mol Pharmacol. 2007;72:1359–1368.

10 Taniguchi T, Inagaki R, Suzuki F, Muramatsu I. Rapid acid extrusion response triggered by α_1 adrenoceptor in CHO cells. J Physiol. 2001;535:107–113.

11 Yamakawa K, Kitamura K, Nonoguchi H, Takasu N, Miller RT, Tomita K. $G_{\alpha 13}$ induces preproET-1 gene expression via JNK. Hypertens Res. 2002;25:427–432.

12 Nishida M, Sato Y, Uemura A, Narita Y, Tozaki-Saitoh H, Nakaya M, et al. $P2Y_6$ receptor-$G\alpha_{12/13}$ signalling in cardiomyocytes triggers pressure overload-induced cardiac fibrosis. EMBO J. 2008; 27:3104–3115.

13 Kitamura K, Shiraishi N, Singer WD, Handlogten ME, Tomita K, Miller RT. Endothelin-B receptors activate $G_{\alpha 13}$. Am J Physiol. 1999;276:C930–C937.

14 Orlowski J, Grinstein S. Na^+/H^+ exchangers of mammalian cells. J Biol Chem. 1997;272:22373–22376.

15 Kenakin T. Differences between natural and recombinant G protein-coupled receptor systems with varying receptor/G protein stoichiometry. Trends Pharmacol Sci. 1997;18:456–464.

Arteriosclerosis, Thrombosis, and Vascular Biology

JOURNAL OF THE AMERICAN HEART ASSOCIATION

American Heart Association®

Learn and Live℠

Histamine Deficiency Decreases Atherosclerosis and Inflammatory Response in Apolipoprotein E Knockout Mice Independently of Serum Cholesterol Level

Ke-Yong Wang, Akihide Tanimoto, Xin Guo, Sohsuke Yamada, Shohei Shimajiri, Yoshitaka Murata, Yan Ding, Masato Tsutsui, Seiya Kato, Teruo Watanabe, Hiroshi Ohtsu, Ken-Ichi Hirano, Kimitoshi Kohno and Yasuyuki Sasaguri

Arterioscler Thromb Vasc Biol published online Jan 27, 2011;
DOI: 10.1161/ATVBAHA.110.215228
Arteriosclerosis, Thrombosis, and Vascular Biology is published by the American Heart Association. 7272 Greenville Avenue, Dallas, TX 72514
 Print ISSN: 1079-5642. Online ISSN: 1524-4636